The Specialist Committee on Ice

Final Report and Recommendations to the 24th ITTC

1. INTRODUCTION

1.1 Membership

The 24th ITTC Specialist Committee on Ice consisted of:

- Dr. Ahmed Derradji-Aouat (Chairman).
  Institute for Ocean Technology, of the National Research Council of Canada, Canada.
- Dr. Jens-Holger Hellmann (Secretary).
  Hamburg Ship Model Basin, Germany.
- Dr. Chang-Kyu Rheem.
  Tokyo University, Japan.
- Dr. Qian-Jin Yue.
  Dalian University of Technology, China.
- Mr. Topi Leiviskä.
  Helsinki University of Technology, Finland.

1.2 Meetings

Three formal meetings of the Committee were held as follows:

- IOT/NRC, Canada, November 2003.
- HSVA, Germany, May 2004.
- DUT, China, February 2005.

2. TASKS FOR THE 24th ITTC ICE SPECIALIST COMMITTEE

The 24th ITTC Specialist Committee on Ice worked on the following five tasks:

Task 1: Develop a Procedure for Experimental Uncertainty Analysis for Ship Resistance in Ice Tank Testing.

Task 2: Review test Procedures and Recommend guidelines, as applicable, for the performance of offshore structures in ice-infested waters.

Task 3: Review of recent developments in the remote sensing and satellite detection of sea ice conditions.

Task 4: Conduct tests to develop an understanding for the performance of open water propellers in ice.

Task 5: Develop a questionnaire and review the numerical methods and computer codes applied to ice engineering.

3. RECOMMENDATION

The 24th ITTC Specialist Committee on Ice worked on the development of one new Procedure (Task 1). The other four tasks (Task 2 to Task 5) were technical investigations.

Thus, there is only one recommendation to the 25th ITTC:

Adopt the new Procedure 7.7020401.1 "Experimental Uncertainty Analysis for Ship Resistance in Ice Tank Testing"

4. STRUCTURE OF THE REPORT

This report is divided into five different sections. Each section covers only one task. A summary for the main conclusions and recommendations are provided at the end of the report.

5. TASK 1: EXPERIMENTAL UNCERTAINTY ANALYSIS FOR SHIP RESISTANCE IN ICE TANK TESTING

5.1 Purpose of Procedure

Develop a methodology to calculate uncertainties in the results of the standard ship resistance in ice tank tests.

5.2 Introduction

Experimental Uncertainty Analysis (EUA) is an analytical process for estimating uncertainties in the results of a given experimental program. Fundamentally, through the EUA process, experimentalists in the laboratory can quantify the agreement (the closeness or the difference) between the measured results and their "true" values.

Historically, until late 1980's, only marginal work on EUA was reported by ocean and marine test facilities. During the 1990's, the International Towing Tank Conference (ITTC) and the International Ship and Offshore Structure Congress (ISSC) have recommended and supported the application of Uncertainty Analysis (UA) in both experimental and numerical/computational fields.

For clarity, in computational and numerical fields, uncertainty analysis is known as Verification and Validation analysis (V&V analysis). The AIAA (1998) gave very useful definitions for the terminology used in V&V analyses. Among these are the definitions for terms such as verification, validation, modelling, simulation, prediction, uncertainty, error, etc. The main objective of V&V analysis is to quantify the uncertainty in the results of a numerical model (or computer simulations). Sources for numerical uncertainties include grid convergence, time step convergence, iterative solution, constitutive model, etc. The main objective of EUA, however, is to quantify the uncertainty in the experimental results obtained in a given test program.

This procedure deals exclusively with Experimental Uncertainties (EU) in the results obtained from resistance tests of model ships in a typical (standard) ice tank. Up to now, in the literature, there are no standards to quantify and/or minimize uncertainties in ice tank ship resistance testing.

Mathematically, the total uncertainty is the geometric sum of two components. They are the systematic component (also, known as the bias uncertainty) and the precision component (also, known as the repeatability uncertainty). The bias component deals with uncertainties in the instrumentation and equipment calibrations (such as load cells, RVDT's[1], yoyo potentiometers and Data Acquisition System (DAS)). However, the precision component deals with environmental and human factors that affect the repeatability of the test results (such as small temperature fluctuations in the ice tank during testing, small misalignments of the ship model in the test set-up, etc).

[1] RVTD = Rotary Variable Differential Transformer

The main objective of this procedure is to provide ice tank experimentalists with a method of analysis to estimate uncertainties in standard ship resistance in ice experiments. To achieve this objective, experiments for ship resistance in ice were conducted using a model for a Canadian Icebreaker "Terry Fox". The results from these tests were used to develop a procedure for EUA in ice tank standard ship resistance tests.

Table 5.1- Test Matrix.

	Ice Sheet #	Model Speed, m/s	Ice Thickness, mm	Ice Strength, kPa
Phase I	**1**	0.1	40	35
	2	0.2	40	35
	3	0.4	40	35
	4	0.6	40	35
Phase II	**5**	0.1	25	35
	6	0.2	25	35
	7	0.4	25	35
	8	0.6	25	35
	9	0.1	55	35
	10	0.2	55	35
	11	0.4	55	35
	12	0.6	55	35
Phase III	**13**	0.1	40	35
	14	0.2	40	35
	15	0.4	40	35
	16	0.6	40	35

5.3 Experimental Data

Experiments for ship model resistance in ice were conducted at the Institute for Ocean Technology of the National Research Council of Canada (www.iot-ito.nrc-cnrc.gc.ca/) using a model scale of the Canadian Icebreaker, "Terry Fox". The model is 3.79 m long (at water line), and it has a maximum beam section of 0.79 m. The model is 1/21.8 scale of the actual icebreaker.

The tests were conducted in three phases (as shown Table 5.1). A brief description of the test program is given as follows:

Phase I tests, test results, and the development of a preliminary method for EUA for ship resistance in ice were documented in two IOT reports (Derradji-Aouat et al., 2002, and Derradji-Aouat, 2002).

The documentation for Phase II test program is also presented in two IOT reports (Derradji-Aouat and Coëffé, 2003, and Derradji-Aouat, 2003). The test matrix in Phase II is the same as that in Phase I (see Table 5.1). The only difference is the target thickness of the ice. In Phase I, all tests were conducted for only one target ice thickness (40 mm), while Phase II tests were conducted for two additional ice thicknesses (25 mm and 55 mm). Together, the two phases provided information for three different ice thicknesses.

In Phase III, the same test matrix as in Phase I was completed. The difference between Phase I and Phase III test programs is that in Phase I, the ship model was attached to the carriage using the tow post while in Phase III, the model was attached to the carriage using the PMM (Planar Motion Mechanism). The details were provided by Derradji-Aouat and van Thiel (2004).

All three phases involved experiments in ice and in open water. A total of sixteen (16) different ice sheets were tested. All experiments in ice were very long test runs. The model was towed at constant speeds throughout the useable length of the ice tank (~ 76 m).

5.4 Experimental Uncertainty Analysis – Basic Equations

The "total uncertainty, *U*" is the geometric sum of a "bias uncertainty, *B*" and a "random uncertainty, *P*". Bias uncertainties (also called systematic uncertainties) are due to uncertainty sources such as load cell calibrations, accuracy of instruments and DAS. Random uncertainties (also called precision or repeatability uncertainties) are a measure of the degree of repeatability in the test results (i.e. if a test was to be repeated several times, would the same results be obtained each time?). Examples for random

uncertainty sources are the changing test environment (such as fluctuations in room temperature during testing), small misalignments in the initial test set-up, human factors, etc.

Mathematically, the total uncertainty is:

$$U = \pm \sqrt{B^2 + P^2} \tag{5.1a}$$

For a single test population (where only one test is performed, and for that one test, n data readings are obtained), random uncertainty "P" from a source "X" is Px:

$$P_X = t * S_X \tag{5.1b}$$

The coefficient "t" is obtained from the standard table for a normal Gaussian distribution (Coleman and Steele, 1998). Its value depends on the desired level of confidence (usually, 95%) and the number of the Degree of Freedom (DOF) in the sample population. The DOF = n –1, where n is the numbers of data readings.

In a multi-test population (where the same test is repeated N times, and each test is represented by only one data point in the population of N data points), the random uncertainty from a source "X" is P_{NX}:

$$P_{NX} = \frac{t * S_{NX}}{\sqrt{N}} \tag{5.1c}$$

Derradji-Aouat (2002) showed that in a typical ice tank ship resistance test, the bias uncertainty component (B) is much smaller than the random one (P), He concluded, therefore, that; in routine ship resistance ice tank testing, the total uncertainty (U) can be taken as equal to the random one. Simply, without a loss of accuracy, the bias uncertainty component can be neglected. It follows that:

$$U = \pm P \tag{5.1d}$$

The above equations are valid for direct measurements (directly measured variables, such as load, deformation, motion, pitch, roll, etc.). In most cases, the measured variables are used to compute engineering parameters (such as stress, strain, resistance, etc.) using Data Reduction Equations (DRE). Additional uncertainties due to the use of DRE need to be considered (as will be discussed later).

The mathematics of this EUA procedure is based on the equations provided by Coleman and Steel (1998). The latter is in harmony with the guidelines of ISO (1995), ASME (PTC-19.1, 1998), and GUM (2003).

5.5 Ship Resistance in Ice

Since the objective of this procedure is to present a methodology to calculate EUA in the results of ship resistance tests in ice tanks, a summary for the standard calculations of ship resistance in ice is given as follows:

The standards for ship resistance in ice (ITTC-4.9-03-03-04.2.1) give the equation for the total resistance in ice, R_t, as the sum of 4 individual components:

$$R_t = R_{br} + R_c + R_b + R_{ow} \tag{5.2a}$$

where,
R_{br} is the resistance component due to breaking the ice, R_c is the component due to clearing the ice, R_b is the component due to buoyancy of the ice, and R_{ow} is the resistance component in open water.

In order to quantify each component, the test plan should include tests in level ice, tests in pre-sawn ice, creeping speed tests, and tests in open water (as per ITTC-4.9-03-03-04.2.1). The open water tests provide values for R_{ow}, while the creeping speed tests give R_b. In the pre-sawn ice tests, $R_{br} = 0$, and therefore:

$$R_t = R_c + R_b + R_{ow} \tag{5.2b}$$

Since R_{ow} and R_b are known (from the open water and the creeping speed tests), thus:

$$R_c = R_t - R_b - R_{ow} \quad (5.2c)$$

where,
R_t, in Eq. 5.2c, is the measured resistance in the pre-sawn ice test runs.

From tests in level ice, the total resistance R_t is measured, and the ice breaking component, R_{br}, is calculated as (from Eq. 5.2a):

$$R_{br} = R_t - R_c - R_b - R_{ow} \quad (5.2d)$$

5.6 EUA – A Procedure For Ice Tank Testing

This procedure was developed on the basis of one hypothesis and one requirement:
- Segmentation hypothesis, and
- Steady state requirement.

Segmentation Hypothesis. To conduct the test program (indicated in Table 5.1), several reasons have contributed to the decision for keeping the speed of the ship model constant throughout most of the useable length of the ice tank (76 m). The main one is the hypothesis that the time history from one long test run can be divided into segments, and each segment can be analysed as a statistically independent test. The hypothesis states that:

"The history for a measured parameter (such as tow force versus time) can be divided into 10 (or more) segments, and each segment is analyzed as a statistically independent test. Therefore, the 10 segments in one long test run are regarded as 10 individual (independent but identical) tests."

Coleman and Steel (1998) reported that, in statistical uncertainty analysis, a population of at least 10 measurements (10 data points) is needed. However, in ice tank testing, conducting the same test 10 times is very costly and very time consuming. Therefore, the principle of segmenting a time history of a measured parameter over a long test run into 10 segments, results in significant savings in costs and efforts. In this case, uncertainties are calculated from the means and standard deviations of the individual segments.

Basically, the hypothesis calls for dividing the long time history into at least 10 equal (more or less equal) segments, calculate the mean and standard deviation for each segment, and then calculate the mean of the means and the standard deviation of the means. An example for segmentation calculations is shown in Table 5.2.

It should be cautioned that the segmentation hypothesis is valid only if the following 3 conditions are satisfied:

- Each segment should span over 1.5 to 2.5 times the length of the ship model,
- Each segment should include at least 10 events for ice breaking (10 ice load peaks),
- General trends (of a measured parameter such as tow force versus time) are repeated in each segment.

Condition 1: is based on the fact that the ITTC Procedure for resistance tests in level ice (ITTC-4.9-03-03-04.2.1) requires that a test run should span over at least 1.5 times the model length. For high model speeds (> 1 m/s), however, the ITTC Procedure requires test spans of 2.5 times the model length.

Condition 2: is based on the fact that in EUA, for an independent test, a population of at least 10 data points is needed to achieve the minimum value for the factor t (in Eq. 5.1). The gain in any further reduction in the value of t, by having more than 10 segments, is minimum (Derradji-Aouat, 2004a).

Condition 3: is introduced to ensure that the overall trends in a measurement are repeated in each segment. This condition serves to provide further assurance into the main hypothesis ("…the 10 segments in one long test run are regarded as 10 individual, independent but identical, tests"). Fundamentally, if the trends are not, reasonably, repeated, then the segments

could not be analysed as "independent but identical" tests.

The time histories measured in creeping speed tests are not subjected to the segmentation hypothesis. Furthermore, it is recognized that the division of the results of a test run into segments is valid only for the steady state portion of the measured data (only the steady state portion of the measured time history is to be used for the segmentation). This is required to eliminate the effects of the initial ship penetration into the ice (transient stage) and the effects of the slowdown and full stop of the carriage during the final stages of the test run (also transient stage).

Steady State Requirement. In ice tank testing, for any given ice sheet, the ice properties are not completely (100%) uniform (same thickness) and homogeneous (same mechanical material properties) all over the ice sheet. This is attributed, mainly, to the ice growing processes and refrigeration system in the ice tank (Derradji-Aouat, 2004b).

In addition to the spatial variability of the material properties of ice, during an ice test run, the carriage speed may (or may not) be maintained at exactly the required nominal constant speed. The control system maintains the carriage speed constant. However, when ice breaks, small fluctuations in carriage speed may take place.

Because of this inherent non-uniformity of ice sheets, the non-homogeneity of ice properties and the small fluctuations in the carriage speed, steady state in the time history of a measurement may not be achieved.

Theoretically, if the time history of a measured parameter is changing, then the segments could not be analysed as "identical" tests. The steady state requirement, therefore, calls for a corrective action to account for the effects of non-uniform ice thickness, non-homogenous ice mechanical properties and small fluctuations in carriage speed on the test measurements.

To identify whether or not the time history for a measured parameter has reached its steady state, the following procedure was applied. The time histories for the measured parameters were plotted along with their linear trend lines (Derradji-Aouat and van Thiel, 2004). A linear trend line with a slope of about zero indicates that a steady state in a measured parameter is achieved.

The non-steady state situation may be attributed to one (or all) of the following 3 factors:

- A changing carriage speed (or small fluctuations in carriage speed) during testing,
- Non-uniform ice thickness,
- Non-uniform mechanical properties of the ice (flexural/compressive strengths, elastic modulus, density of ice, etc.).

The contribution of each factor was investigated by Derradji Aouat and van Thiel (2004), and they concluded that the effect of changing carriage speed can be ignored (that is factor # 1). The effects of the other two factors are given as:

Non-Uniform Ice Thickness: Mean ice thickness profiles were calculated, each mean profile is the average of 3 measured ice thickness profiles. Each profile is a series of ice thickness measurements (every 2 m) along the length of the ice tank.

The linear trend lines, through the mean thickness profiles, indicate that the ice thickness varied within a range of 0.69% to 2.64%.

To correct for the effects of non-uniform ice thickness on the resistance measurements, the following rational was followed.

The ice thickness corrections are applied only to the resistance due to the ice. Therefore,

the total ice resistance ($R_{\text{Total Ice}}$) is equal to the measured resistance in the ice tests (R_{Measured}) minus the resistance measured in the open water tests ($R_{\text{Open Water}}$).

$$\left(R_{\text{Total}-\text{ice}}\right)=\left(R_{\text{Measured}}\right)-\left(R_{\text{Open}-\text{Water}}\right) \qquad (5.3a)$$

To correct for the ice thickness, the following equation is used:

$$\left(R_{\text{Total}-\text{ice}}\right)_{\text{correct}}=\left(R_{\text{Total}-\text{ice}}\right)*\frac{h_0}{h_m} \qquad (5.3b)$$

where,
$(R_{\text{Total-ice}})_{\text{correct}}$ is the corrected total ice resistance, $(R_{\text{Total-ice}})$ is the measured total ice resistance (Eq. 5.3a), h_0 is the nominal ice thickness, and h_m is the measured ice thickness.

The time histories measured in the creeping speed test runs are not subjected to corrections for ice thickness variation. The length of each creeping speed test run is small (only one ship length ≈ 3.8 m), the variation of ice thickness over this small length can be ignored.

Non-Homogeneous Ice Properties: Mean flexural strength profiles along the length of the ice tank were given by Derradji-Aouat and van Thiel (2004). Typically, the flexural strength profiles are obtained using in-situ cantilever beam tests. The beam dimensions have the proportions of 1:2:5 (thickness, h_f,: width, w: length, L). The flexural strength σ_f is calculated as:

$$\sigma_{\text{f}}=\frac{6PL}{wh_{\text{f}}{}^2} \qquad (5.4a)$$

where,
P is the applied point load.

The uncertainty in the flexural strength is:

$$U\sigma_{\text{f}}=\sqrt{U_{\text{P}}^2+U_L^2+U_W^2+2U_{hf}^2} \qquad (5.4b)$$

where,
U_L, U_W, and U_{hf} are the uncertainties in the measured dimensions (L, w and h_f). U_p is the uncertainty in the measured point load.

Derradji-Aouat (2002) reported that any data correction for ice thickness includes, implicitly, the correction for the flexural strength of the ice. This is due to the fact that ice thickness is a fundamental measurement while the flexural strength is a calculated material property (flexural strength is calculated from measurements of applied point load and dimensions of the ice cantilever beam). Since this work deals with EUA of actual "fundamental" measurements, it is recognized that if corrections were to be made for both ice thickness and flexural strength, double correction (double counting) would take place, and the final uncertainty values would be overestimated. The same argument is valid for corrections for the comprehensive strength of ice (the latter is calculated from applied axial load and measurements of actual dimensions of the ice sample).

Measured ice density profiles along the length of the ice tank were also given by Derradji-Aouat and van Thiel (2004). The density of ice, ρ_i, is given as:

$$\rho_{\text{i}}=\rho_{\text{w}}-\frac{M}{V} \qquad (5.4c)$$

where,
ρ_w is the density of water. M is the mass of the ice sample.

The volume, V, is calculated from the sample dimensions (length, L, width, W, and thickness, H): The uncertainty in the ice density is:

$$U_{\rho i}=\sqrt{U_H^2+U_L^2+U_W^2+U_M^2} \qquad (5.4d)$$

During testing, it was noted that the variation of density along the centre line of the tank varied between 4.58% and 8.60%.

5.7 Calculations of Random Uncertainties

In the following example, the discussion will be focused on the results given in Fig. 5.1. Other examples were given by Derradji-Aouat et al. (2004). Figure 5.1a is the measured tow force time history a resistance test in level ice at model speed of 0.1 m/s. Fig. 5.1b shows examples for the segments, in this particular test, the time history was divided into 15 segments. Table 5.2 shows the segments for the mean tow force history; all ice sheets in Phase I are presented. The tow force history in each test is divided into > 10 segments. Mean tow force (F_{T_mean}) is obtained for each segment.

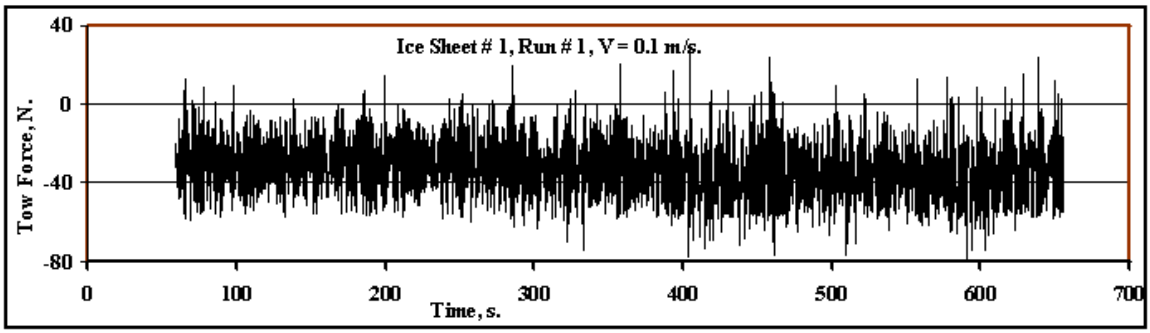

Figure 5.1a- An example for typical test measurement - Tow force versus time (Constant speed, v = 0.1 m/s, level ice, ice thickness = 40 mm, length of run = 65 m).

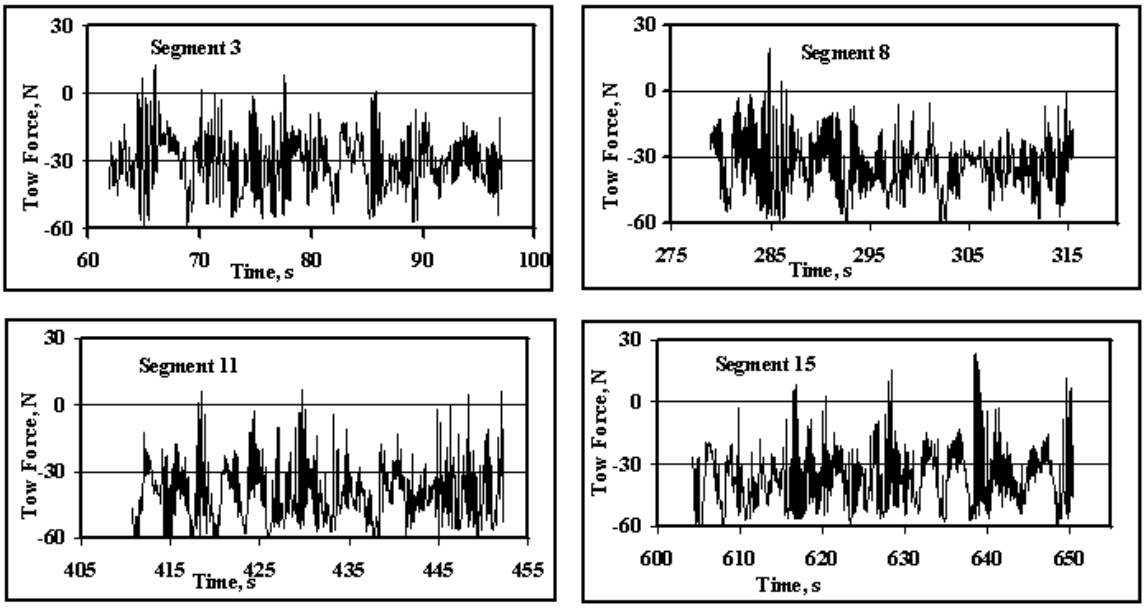

Figure 5.1b- Division of measured test results (in Fig. 5.1a) into segments (4 segments are shown as examples).

For each time history, the mean of the > 10 means (Mean_F_{T_mean}) and the standard deviation of the 10 means (STD_F_{T_mean}) were calculated (as shown in Table 5.2).

Random uncertainties in the tow forces $U(F_{T\_mean})$ are calculated in three (3) steps:

Step 1: In Table 5.2, after the calculations of the mean of means and standard deviation of means, the Chauvenet's criterion is applied to identify outliers (outliers are discarded data points). The Chauvenet number for mean tow forces is $(\text{Chauv }\#)_{Mean}$:

$$(Chauv\ \#)_{\text{Mean}} = \left| \frac{F_{\text{T\_mean}} - \left(Mean\_F_{\text{T\_mean}} \right)}{\left(STD\_F_{\text{T\_mean}} \right)} \right| \qquad (5.5a)$$

For 10 to 15 segments, the Chauv # should not exceed 1.96 to 2.13. In Table 5.2, data points with Chauv # greater than 1.96 were disregarded. A new mean of means and a new standard deviation of means are calculated from the remaining data points (Table 5.2).

Table 5.2- Examples for calculations for random uncertainties in mean tow force.

Mean Tow Force, Continuous Ice Sheet - RUN # 1									
Ice Sheet #	Segment #	TF-mean (N)	Mean (TF_mean)	STD_mean (N)	(Chauv#)	New Mean TF_mean	New STD_mean	Uncertainty Value (N)	Uncertainty %
1	3	-30.45	34.67	0.88	1.54			0.49	1.41%
	4	-30.49	34.67	0.88	1.28				
	5	-29.88	34.67	0.88	1.03				
	6	-30.63	34.67	0.88	0.77				
	7	-31.69	34.67	0.88	0.51				
	8	-34.03	34.67	0.88	0.26				
	9	-32.91	34.67	0.88	0.00				
	10	-35.80	34.67	0.88	0.26				
	11	-40.16	34.67	0.88	0.51				
	12	-38.19	34.67	0.88	0.77				
	13	-38.23	34.67	0.88	1.03				
	14	-40.24	34.67	0.88	1.28				
	15	-36.26	34.67	0.88	1.54				
2	3	-42.80	36.57	0.27	1.55			0.14	0.39%
	4	-44.29	36.57	0.27	1.31				
	5	-42.40	36.57	0.27	1.08				
	6	-45.13	36.57	0.27	0.84				
	7	-44.51	36.57	0.27	0.60				
	8	-43.25	36.57	0.27	0.36				
	9	-44.30	36.57	0.27	0.12				
	10	-45.43	36.57	0.27	0.12				
	11	-47.42	36.57	0.27	0.36				
	12	-46.87	36.57	0.27	0.60				
	13	-47.57	36.57	0.27	0.84				
	14	-47.82	36.57	0.27	1.08				
	15	-51.21	36.57	0.27	1.31				
	16	-50.96	36.57	0.27	1.55				
3	3	-54.79	48.74	0.47	1.53			0.27	0.56%
	4	-56.09	48.74	0.47	1.25				
	5	-53.44	48.74	0.47	0.97				
	6	-53.90	48.74	0.47	0.69				
	7	-55.66	48.74	0.47	0.42				
	8	-49.25	48.74	0.47	0.14				
	9	-56.16	48.74	0.47	0.14				
	10	-54.26	48.74	0.47	0.42				
	11	-62.24	48.74	0.47	0.69				
	12	-60.64	48.74	0.47	0.97				
	13	-60.51	48.74	0.47	1.25				
	14	-60.96	48.74	0.47	1.53				
4	3	-60.84	61.77	0.89	1.51			0.54	0.87%
	4	-60.17	61.77	0.89	1.21				
	5	-62.57	61.77	0.89	0.90				
	6	-61.22	61.77	0.89	0.60				
	7	-60.53	61.77	0.89	0.30				
	8	-62.17	61.77	0.89	0.00				
	9	-65.25	61.77	0.89	0.30				
	10	-67.83	61.77	0.89	0.60				
	11	-66.28	61.77	0.89	0.90				
	12	-67.63	61.77	0.89	1.21				
	13	-69.09	61.77	0.89	1.51				

Note: Calculations for all other test runs were given by Derradji-Aouat (2004b). Note that the segment # starts always as # 3. During testing and data acquisition, segment # 1 was designated for the raw data and segment # 2 was designated for the tarred data.

Step 2: After calculating the new mean of the means and the new standard deviation of the means (from the remaining segments), random uncertainty in the mean tow force is:

$$\left(U(F_{\mathrm{T\_mean}})\right) = \frac{t^{*}\left(STD\_F_{\mathrm{T\_mean}}\right)}{\sqrt{N}} \qquad (5.5b)$$

where,
$t \approx 2$, and N is the number of the remaining data points (valid segments).

Step 3: Random uncertainties are expressed in terms of uncertainty percentage (UP):

$$\left(U_{\mathrm{P}}(F_{\mathrm{T\_mean}})\right) = \frac{U(F_{\mathrm{T\_mean}})}{Mean\_F_{\mathrm{T\_mean}}} * 100 \qquad (5.5c)$$

It is important to note that the above procedure (segmentation of the measured time history, checks for the steady state requirement, correction for ice thickness, the use of the three calculation steps) is valid for calculating random uncertainties in all other measured ship motion parameters (such as pitch, heave, yaw and sway).

5.8 Effects of Data Reduction Equations

Equation 5.3b was proposed to correct for the effects of ice thickness variations on the values of random uncertainties in resistance. It should be recognized that the corrected resistance curves are not direct laboratory measurements, but they are calculated from the analytical Eq. 5.3b. The process of using analytical equations to correct measured parameters is called: "Application of Data Reduction Equations, DRE".

In EUA, there are additional random uncertainties involved in using DRE. The uncertainty involved in using Eq. 5.3b is:

$$\left(\frac{U_R}{R}\right) = \left(\left(\frac{U_{R_0}}{R_0}\right)^2 + \left(\frac{U_h}{h_0}\right)^2\right)^{\frac{1}{2}} \qquad (5.6)$$

In the above equation, (U_R/R) is the total uncertainty in resistance. Both (U_{R0}/R_0) and (U_h/h_0) are the relative uncertainty in the measured ice resistance and the relative uncertainty in the measured ice thickness, respectively. In Eq. 5.6, the value of (U_h/h_0) is an additional relative uncertainty that is induced to account for the use of the DRE.

5.9 Calculations of Bias Uncertainties

Sources for Bias Uncertainties. Bias uncertainties are attributed to the DAS and the instrumentation used for measurements (such as load cells, yoyo potentiometers and RVTD's). Table 5.3 is an example for how bias uncertainties are calculated. The first column of Table 5.3 is a list of the major bias uncertainty sources involved. Essentially, the list was developed by the DAS system specialists, electronics and instrumentation technologists. The experience and skills of these professionals play a significant and critical role in identifying major sources for uncertainties. Typically, calculations of bias uncertainties are based on the instrument data sheets, load cell calibration curves and DAS manufacturer design and gain specifications (details are given by Derradji-Aouat (2002)).

Determination of Bias Uncertainties in Ice Tank Testing. As shown in Table 5.3, the DAS on board of the ice tank carriage comprises three main sub-components: The amplifier, the multiplier and the Daq-board. The instrumentation used for measurements included a load cell (to measure tow force), a yoyo potentiometers (to measure heave) and two RVDT's to measure pitch and roll of the model. The carriage speed was measured automatically via a dedicated channel in the carriage control system.

The results (in Table 5.3) show that the sum of all bias uncertainties for any given instrument is below 0.4%.

5.10 Calculations of Total Uncertainties

In ice tank experiments, bias uncertainties are much smaller than the random once. Subsequently, it is recommended that; in ice tank testing and without a loss of accuracy of the uncertainty analysis, the total uncertainty can be taken as equal to the random one (Eq. 5.1d). Simply, the bias uncertainty component can be neglected (Derradji-Aouat et al., 2004).

Table 5.3- Ice tank bias uncertainty calculations.

Transducer Type	Load Cell	YoYo Pot	RVDT	RVDT	Carriage
Parameter	Tow Force (N)	Sinkage (m)	Pitch (degrees)	Roll (degrees)	Speed (m/s)
DAS Channel	CH. 8	CH. 21	CH. 27	CH. 28	CH. 33
Transducer	% F.S.	% F.S.	% F.S.	% F.S.	% F.S.
Non Linearity	0.0200		0.1870	0.1930	
Histerisis	0.0200				
Non Repeatability	0.0100		0.0200	0.0200	
Zero Offset Drift	0.0216	0.0432			
Span Temp. Coefficient		0.0432	0.2160	0.2160	
Accuracy		0.1500			
DAS- NEFF Amplifier	% F.S.	% F.S.	% F.S.	% F.S.	% F.S.
Gain Stability	0.0350	0.0350	0.0350	0.0350	0.0350
Non Linearity	0.0200	0.0200	0.0200	0.0200	0.0200
Zero Stability	0.0160	0.0030	0.0030	0.0030	0.0030
Zero Drift	0.0220	0.0130	0.0130	0.0130	0.0130
Common-Mode Rejection	0.0500				
DAS-Iotech DBK12 Multiplexer	% F.S.	% F.S.	% F.S.	% F.S.	% F.S.
Gain Accuracy	0.2500	0.2500	0.2500	0.2500	0.2500
Non Linearity	0.0150	0.0150	0.0150	0.0150	0.0150
Offset Drift	0.0250	0.0250	0.0250	0.0250	0.0250
Common-Mode Voltage	0.0020	0.0020	0.0020	0.0020	0.0020
DAS Iotech Duqboard/200	% F.S.	% F.S.	% F.S.	% F.S.	% F.S.
A/D Linearity	0.0031	0.0031	0.0031	0.0031	0.0031
A/D Zero Drift	0.0050	0.0050	0.0050	0.0050	0.0050
A/D Gain Drift	0.0150	0.0150	0.0150	0.0150	0.0150
Analogue i/p Resolution	0.0015	0.0015	0.0015	0.0015	0.0015
Analogue i/p Accuracy	0.0250	0.0250	0.0250	0.0250	0.0250
Analogue i/p Gain Temp. Coefficient	0.0015	0.0015	0.0015	0.0015	0.0015
Analogue i/p Offset Temp. Coefficient	0.0012	0.0012	0.0012	0.0012	0.0012
TOTAL BIAS (SYSTEM) UNCERTAINTY %	% F.S.	% F.S.	% F.S.	% F.S.	% F.S.
Fs = Full Scale	0.2655	0.3038	0.3848	0.3878	0.2570

Note: Total bias uncertainty values are the same for all test runs since the same DAS and same transducers are in all test runs (an all test types: in ice or in open water).

5.11 Summary of Procedure

To compute the uncertainties in the results of a ship resistance in ice test program, the following procedure should be followed:

- Perform one test for ship resistance in ice. The test run should be long enough so that it can be divided into 10 segments (satisfying the 3 conditions given in Section 5.6.1).
- Check the measured resistance time history

for the steady state requirement (satisfying the requirement in Section 5.6.2).

- Apply the segmentation (at least 10 segments should be obtained, as shown in Fig. 5.1 and Table 5.1).
- Correct the resistance for the variation of ice thickness (using Eq. 5.3b).
- Use the three steps to calculate random uncertainties (using Eqs. 5.5a, 5.5b and 5.5c).
- Estimate bias uncertainties using calibration data and components data sheets, as shown in Table 5.3.
- Calculate total uncertainties using Eq. 5.1a (or 5.1b if bias uncertainties are neglected).
- Correct for the application of any DRE (using Eq. 5.6).

5.12 Validation

Test Results and Comparisons. In the three phases of testing, uncertainty values varied between 3% and 10% (Derradji-Aouat et al., 2004).

The 23rd ITTC Specialist Committee on Ice presented an example for how to estimate random uncertainties in ice testing. In that example, the Committee used the results of tests for ship resistance conducted by Kitagawa et. al, (1991 and 1993) in the Japanese NMRI ice tank. Comparisons between the calculations presented by the 23rd ITTC and those reported in the present test program resulted in the following conclusions:

Although the calculations of uncertainties were performed using the results of two different test programs, conducted at two different ice tanks in two different countries (Canada and Japan) and about 10 to 12 years apart, the final calculations converged to about the same range of uncertainties (3% to 10%).

The range of uncertainty (3% to 10%) is not far from the range (10% to 12%) reported by Newberry (1992), using a different ship model (R class icebreaker), 12 years ago, at the IMD ice tank.

It should be recognized that more EUA comparisons using data from various ice tanks (various model ice types and test conditions) are very much needed to accurately estimate and compare uncertainties involved in various tanks. At this point in time, the limited number of EUA publications, in the literature of ice tank testing, inhibited the work towards a larger and more comprehensive comparison study in uncertainties among tanks worldwide (only qualitative comparisons are possible).

5.13 Benchmark Tests

Kitagawa H., Izumiyama K., Koyama K., and Uto S. (1991). A study on ice tank experimentation (PART-1). POAC-1991.

Kitagawa H., Izumiyama K., Koyama K., and Uto S. (1993). A study on ice tank experimentation (PART-2). POAC-1993, pp. 889 – 900.

Newbury S. (1992): Realibility of resistance experiments in ice with 1:20 Scale Model of the Canadian R-Class Icebreaker. NRC/IMD report No. LM-1992-10.

6. TASK 2: REVIEW OF CURRENT TEST PRACTICES FOR THE PERFORMANCE OF OFFSHORE STRUCTURES IN ICE

6.1 Introduction

Since the 1960s, a large number of small-scale laboratory tests and full-scale field tests have been conducted to determine the magnitude of the forces excreted by ice on offshore structures. However, due to the complexity of ice-structure interaction processes, many uncertainties exist in using the existing methods to determine ice loads.

The purpose of this report is to review the existing testing methods aimed at determining ice loads on offshore structures.

By and large, ice load testing methods can be classified into small-scale laboratory tests using laboratory ice and model structures, full-scale tests, and in-situ tests using actual offshore structures and ice conditions.

The main advantage of small-scale structure models tested in the laboratory is that the test set up and the test environmental parameters can be controlled. However, up to now, not all scaling issues are resolved; especially testing to simulate dynamic ice structure interactions. The main disadvantage of field-testing is that the parameters are not controlled.

In the following, existing test procedures in both laboratory and field are reviewed. A general presentation regarding the current state and knowledge for determining ice loads on offshore structures is presented.

6.2 Classification of Forces and Structures

The magnitude of the force excreted by ice on an offshore structure depends strongly on the mode of failure of ice and its clearing process during its interactions with the structure. The structure itself can be vertical or sloped. Also, it can be cylindrical, conical, prism, etc. Thus, it is necessary to classify ice forces according the nature of the excreted ice loads (static, quasi-static, dynamic, etc), and the characteristics the of the ice-structure interaction process (failure mode and behaviour of ice).

Classification of Ice forces.

- Static Ice Force: The driving force of the ice sheet is very slow (such as temperature variations or very slow wind or current speed). This is low rate loading conditions and the ice force is without period.
- Quasi-Static Ice Force: The ice sheet has an apparent speed (not very slow). However, inertial forces and/or the period of ice forces can be neglected.
- Dynamic Ice Force: The inertial forces and/or the period of the ice force can not be neglected; they even have an apparent effect on the response of the structure. For example, in some cases, during the impact of an ice sheet with a structure, the ice force can be very dominant, especially if the period of ice force is close to the period of the structure (resonance of vibration may take place).
- Global ice force: Total force of ice acting on the entire structure.
- Local ice force: Global ice forces are transferred to the structure via local areas. The force acting on a local area is called local ice force.

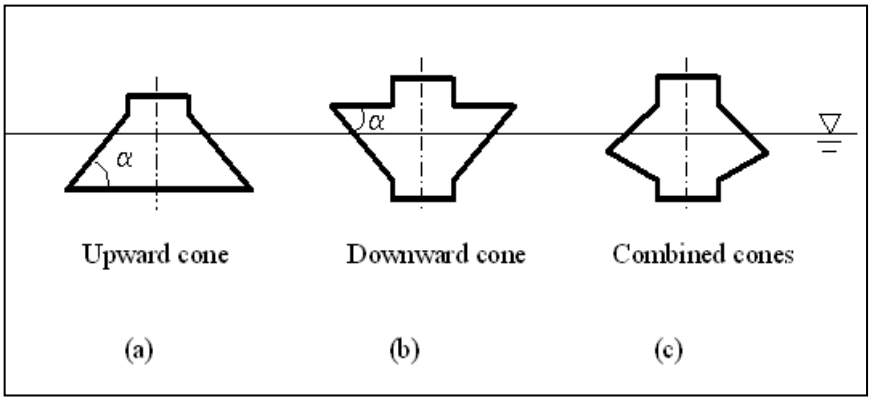

Figure 6.1- Typical ice breaking cones.

Classification of Structures.

- Vertical structures: The face of the structure is perpendicular to the ice sheet. The main mode of failure of ice is crushing. The intensity of the ice force is limited by its compressive strength.

- Sloping structures: Sloping surfaces may be an integral part of the structural design or deliberately added onto an existing structure. Sloping structures favour bending ice failure, rather than crushing. Thus, lesser ice loads are obtained. For actual designs, the sloping surface can be upward or downward sloping surfaces (examples of a conical structures is given in Fig. 6.1).
- Wide structures: The width of the structure is much larger than the wide of the ice sheet. When ice acts on wide structures, often ice ridges form in front of the structure. Thus, in the calculations of ice loads, the effects of the ice ridges should be considered.
- Narrow structures: The width of ice sheet is the in same order as (or larger than) the wide of the structure. The broken ice can easily be cleared up from the sides of the structure. Repeated ice breaking and clearing process take place.
- Compliant structure: The structure undergoes considerable deformation under the action of ice forces. If the fundamental frequency is close to the frequency of ice breaking, dynamic amplification becomes significant.

6.3 Full-Scale Tests

The main advantage of full-scale tests is the elimination of the scaling law effects. The disadvantage, however, is that it is very hard to get a complete information regarding ice forces, since it is not a controlled environment. Over the years, full-scale tests have been conducted on jacket platforms, fixed gravity structures, lighthouses, man-made islands, etc.

Ice behaviour affects significantly the magnitude of ice loads. Full-scale tests show that when ice acts on vertical structures in crushing mode of failure, three different types of failure mode take place: Depending on the speed, they are the ductile, the brittle, and the ductile-brittle transition failure. The three modes of failure result in different ice load intensities (Yue, 2002)

In general, ice forces can be measured directly (using load cells) or it can be estimated from the deformation of the structure and ice properties (such as ice thickness, ice speed, ice strength, etc.)

Measuring Ice Forces by Load Panels. Measuring ice forces by installing ice load panels at the water level is a direct ice force measurement. Properly designed ice load panels will be used also to measure the magnitude of the ice force and to collect a record for the ice load time history.

Figure 6.2a- Load panel for cylindrical structures.

Figure 6.2b- Load panel for conical structures.

Ice load panels contain one or more elastic elements; which transfers the force into the recording instrumentation. The surface of the panel should have the same geometric configuration as the actual structure.

The size of a typical ice load panel is about 1 to 2 m wide. Note that load panels lend themselves effectively to measure local ice loads. To measure global ice forces, a group of panels can be combined together and used as a bundle, while conserving the original shape of the structure. Fig. 6.2 shows examples for two ice load panels. The first panel was designed for a cylindrical structure, while the second was designed for a conical structure.

The stiffness of the load panel is an important parameter. Essentially, the fundamental frequency of the panel should be much higher than the frequency of the ice force breaking.

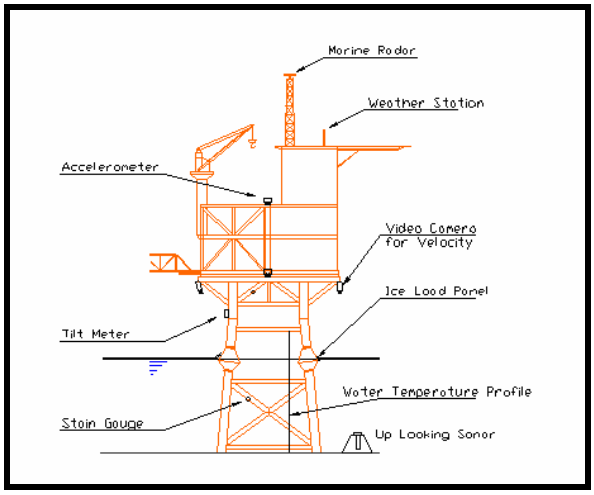

Figure 6.3- Example of a full-scale test set up.

Measuring Ice Forces by Structural Response. The deformation "displacement" of the structure can be used to determine ice forces. In this case, the structure is viewed as a transducer. Figure 6.3 shows an example for a typical full-scale test set up, where the objective is to use the structural deformation to determine the magnitude of global ice forces. Generally, prototype structures are complex systems, and the Finite Elements Method "FEM" and/or in-situ calibration techniques are used to determine the relation between the ice force and the structural response.

Dynamic Response of the Structure. For compliant structures under ice actions, dynamic response of the structure can be induced. Accelerometers are used to record the dynamic displacements and accelerations.

Deflection of the Structure. The total deflection of the structure can be used to determine global ice forces. However, it is not a trivial task to measure accurately the deflections of an actual offshore structure. FEM" and/or in-situ calibration techniques are used to determine the relation between the global ice force and the structural deflection.

Full-scale tests show that when ice acts on vertical structures in crushing mode of failure, three different types of failure mode take place: Depending on the speed, they are the ductile, the brittle, and the ductile-brittle transition failure. The three modes of failure result in different ice load intensities (Yue, 2002)

Ice Properties. The main factors influencing the magnitude of ice loads are: ice thickness, ice speed, and ice strength.

Ice Thickness: When ice interacts with vertical structures in crushing mode of failure, we cannot observe ice thickness directly. We need to use other methods such as Up Looking Sonars (ULS). If the ice sheet breaks in bending, we can use video cameras to record the ice thickness.

Ice Velocity: Ice forces are very sensitive to the speed of the ice floe. When ice acts on vertical structures in crushing mode of failure, the strength of ice is sensitive to the speed (rate dependent). If ice interacts with compliant structure, the dynamic ice force is function of ice speed. The ice speed measurement can also be obtained using video cameras.

Ice Strength: Ice forces depend on the corresponding mode of failure (bending, crushing, shear, etc). Ice strength can be estimated from ice properties, such as salinity, density, and temperature.

6.4 Small-Scale Laboratory Tests

The main advantage of small-scale tests in ice tanks and cold rooms is that the test set up and the ice environmental parameters can be controlled. The dimensions of the facility, the capacity of loading, the size of the model structure, ice strength, and ice thickness are reduced (smaller – model size). Theoretically, the results of small-scale tests can be extrapolated through scaling laws into full-scale scenarios. In practice, however, there are many scaling law problems with respect to dynamic ice loads. Fundamentally, scaling laws are valid for linear elastic problems. However, for a highly dynamic behaviour that involves fracture and damage of ice, the validity of applying existing scaling laws is uncertain.

Originally, existing ice basins were designed to study ship resistance in ice. The model ship is fixed to the carriage, and the carriage moves at a prescribed speed through the ice sheet. For fixed offshore structures, this is applicable to static load measurements of ice loads. However, for dynamic ice force measurements, many uncertainties are involved.

Several factors limit the size of the model structure and the ice thickness. Most laboratories are large, but their capacity to model large size structures in ice is limited.

Model Structures. In ice tanks, the model structure is fixed to the carriage. The carriage moves at a given speed and pushes the structure through the ice sheet. If the model structure is rigid, and the objective of the tests is to measure static or quasi-static ice forces, the errors induced are relatively small. But, for investigating dynamic ice structure interactions, the above model-carriage set up is very questionable.

In some cases, the structure is fixed and the ice sheet is pushed. This fixed model structure set up satisfies the dynamic modelling requirements, such as ice mass, stiffness and damping. However, high capacity actuators are needed to push the entire ice against the structure. Figure 6.4 is an example for a small-scale test set up, where the ice sheet is pushed against a fixed model structure.

The stiffness and the fundamental frequency of the model structure are very important to the breaking frequency of the ice. If the natural frequency of the structure is close to the frequency of ice breaking, dynamic amplification will be significant. For tests with the objective to determine static ice forces, it is suggested that the natural frequency of the model structure should be much higher than the breaking frequency of the ice

For tests with the objective to determine dynamic ice forces, a compliant model structure is needed. In this case, the breaking frequency of the ice and the breaking length become important factors. Using compliant model structures with known natural frequencies (fs), the breaking frequency of ice (fi) at different speeds (Vi), the breaking length of the ice L_b can be determined as:

$$f_S = f_i = \frac{V_i}{L_b} \tag{6.1}$$

In the low speed range, the amplitude of the structure increases with the speed of ice. In high-speed range, the amplitude of the structure decreases with ice speed. The transition point means that at that speed the breaking frequency of ice sheet is equal to the natural frequency of the structure (Yue, 2002)

In actual structures, the top mass and top stiffness are very large. But, in small-scale test it is very difficult to satisfy the scaling laws. In most small-scale tests, the natural frequency of the model structure has the same value as the real structure, but the stiffness and mass are much smaller than those of the real structure. This may result in structural response much different than the real structure.

Model Ice. In ice tanks, the ice thickness, the elastic properties and the strength of ice are reduced to model size. Many laboratories adopted the use "model ice", this is fresh water doped with various chemicals. Other laboratories use sea -water to make ice.

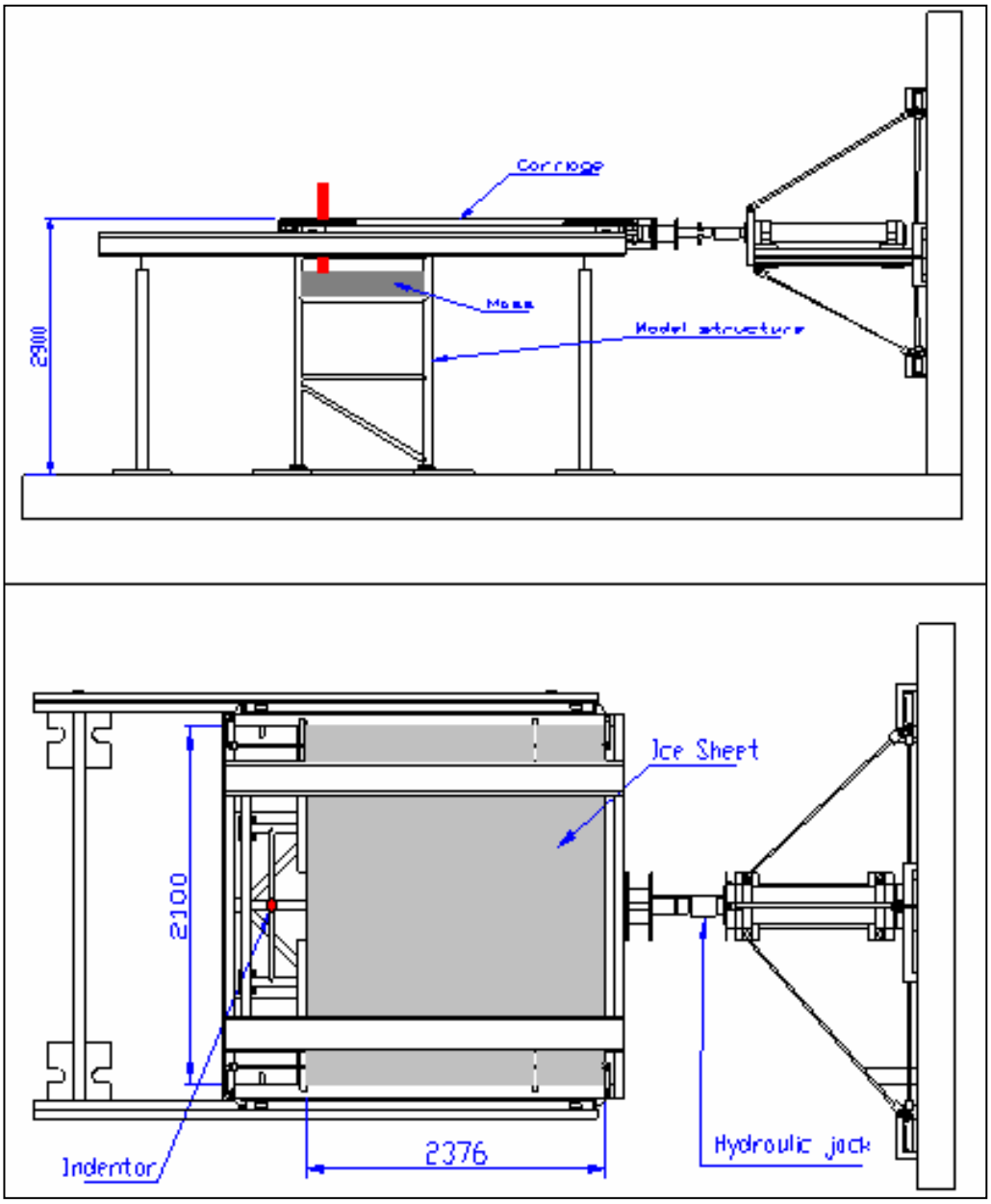

Figure 6.4- Active loading small-scale set up in a cold room at DUT (Top View).

7. TASK 3: REVIEW OF RECENT DEVELOPMENTS IN REMOTE SENSING AND SATELLITE DETECTION OF SEA ICE

Sea ice information is indispensable to ships and offshore structures in ice covered waters. The sea ice condition is the most important parameter for design of icebreakers and offshore structures to be installed in ice covered seas. It would also be the most important information for making a decision to select the shipping route and the navigation of ships in ice covered seas. Satellite remote sensing is the most powerful technique to collect sea ice information. The advantage of satellite remote

sensing is the fact that data from large (and/or inaccessible) areas can be obtained rapidly. Also, some systems can function at night or through fog, cloud or rain. This latter point is especially valuable for polar remote sensing, since these regions undergo six-month nights and are typically cloud-covered.

7.1 Electromagnetic Properties and Satellite Images of Sea Ice

The first of these properties is the reflectivity (or albedo), which measures the radiation reflected from the surface and below it (volume scattering - Fig. 7.1). If volume scattering is significant, we also need to consider the penetration length (or depth), which defines the maximum distance below the surface from which significant amounts of radiation are scattered. For active microwave remote sensing, a concept analogous to the reflectivity is defined. This is the normalized dimensionless backscattering coefficient, usually just called the backscattering coefficient. This also measures the reflecting ability of the material, but it is normally expressed with an explicit statement of the incident angle and state of polarization of the radiation to which it applies. Finally, for thermal remote sensing in both the thermal- infrared (TIR) and passive microwave bands, the important quantity is the emissivity, which relates the power emitted by a real material to the theoretical maximum emitted by a perfect emitter (a black body under identical condition and at the same physical temperature). Naturally occurring objects all have an emissivity of less than 1. All of these electromagnetic properties are in general defined as a function of wavelength or frequency, since they are not in general constant across a waveband (Massom, 1991).

7.2 Visible (VIS) and Near-Infrared (NrIR) Observations

Remote sensing in the VIS and NrIR parts of the electromagnetic spectrum relies on the sun as a source of illumination. Illumination angles change as a function of time, season and latitude. In the VIS, the nature and intensity of the reflected radiation as measured by the sensor are a product of the incident radiation and the absorption, scattering and reflectance properties of the target medium. The penetration depth is negligible at such short wavelengths, and absorption and scattering processes are concentrated within the uppermost few millimetres of surface layer. The scattering is a function of geometric properties of the surface and the absorption coefficient, which is a function of wavelength.

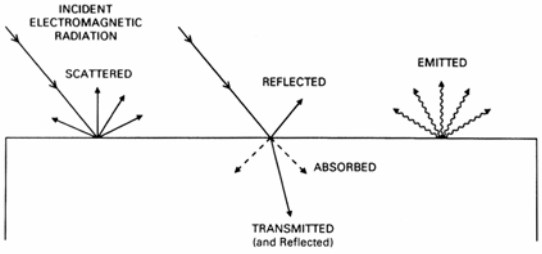

Figure 7.1- Interaction mechanisms between electromagnetic radiation and matter. Specular scattering predominates from surfaces which are smooth relative to the wavelength of the incident radiation; diffuse scattering predominates from rough surfaces. Both are dependent on incidence angle (Rees, 1990).

Albedo (reflectance) is an important snow and ice bulk parameter that can be measured at short (VIS and NrIR) wavelengths. The albedo of snow is much greater than that of any other common natural substance at these wavelengths. Spectral variations in the reflectance of ice at VIS and NrIR wavelengths are mainly due to the fact that the absorption coefficient of these surfaces varies by up to seven orders of magnitude at wavelengths between 0.4 m and 2.5 m. Ice and water are optically very similar, except for the region from 1.55 - 1.75 m where ice is slightly more absorptive. In the NrIR wavelengths, ice is moderately absorptive, and the absorption increases with wavelength. The albedo is higher at VIS wavelengths for thicker sea ice, whereas it is insensitive to ice thickness in the NrIR. Albedo increases with a decrease

in ice density, due to multiple scattering by the air bubbles. The faster sea ice grows, the higher its albedo. Moreover, sea ice is typically covered with snow covers of differing ages and states.

Figure 7.2a- SPOT-2 (JAXA)

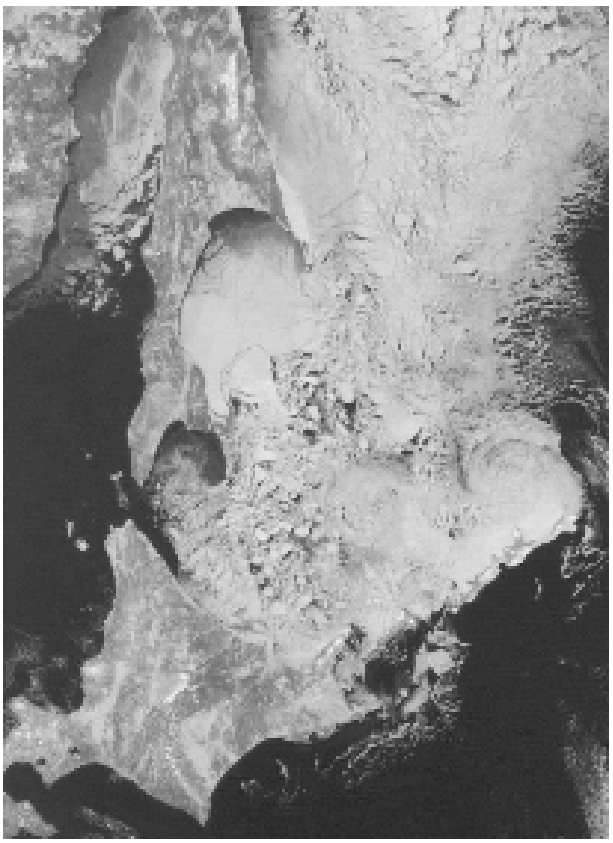

Figure 7.2b- AVHRR, NOAA

Figure 7.2- Sea ice of VIS satellite images in Okhotsk Sea.

7.3 Thermal Infrared Observations

The important parameters in TIR (wavelength 2-15 m) remote sensing are the emissivity of a material and the penetration length. The former determines the efficiency of the material at emitting thermal radiation, the latter the depth below the surface from which this radiation emanates. Penetration depth in all the important geophysical materials in polar remote sensing (ice, snow and water) are very small at TIR wavelengths, so that the signals detected from space are derived only from the surface and near-surface layer. Emissivities are typically high (0.97-1.00), so that most of the variation in the detected signal is caused by real temperature differences rather than by differences in the target material.

In the 3-5m region, the energy detected by a satellite sensor represents a mixture of solar reflected and thermally emitted energy; for this reason, this window is normally used for environmental purposes only when measurements are made at night. Neither this nor the 10.5-12.5m atmospheric windows is perfectly transparent.

Presently available TIR detectors are characterized by a lower spatial resolution and longer dwell time than VIS and NrIR sensors, and the detectors need to be cooled to about 115K in order to reduce thermal noise. In practice, the interpretation of thermal data and images of areal temperature distribution over snow and ice is far from simple, as the measured radiance depends on the emissivity of the surface and atmospheric effects. The contribution of the latter can be great in Polar Regions. Thus, some knowledge of the physical and temporal conditions under which the surface is heated is essential in analysing such data. Differences in reflectance, emissivity and thermal inertia of the target media and variable atmospheric radiance are important factors affecting the observed surface temperatures.

Unfortunately, the usefulness of VIS and NrIR remote sensing of polar regions is

severely limited by its inability to penetrate cloud cover and darkness, and that of TIR sensing by its inability to penetrate clouds. The ability of the latter to penetrate darkness is, however, a considerable advantage.

7.4 Passive Microwave Observations

Passive microwave sensors detect radiation originating by the same thermal mechanism as TIR radiation, but at much longer wavelengths. The important electromagnetic parameters are again the emissivity and the penetration length, but in this case the variability is much greater, and strongly influenced by nature and condition of the target material.

The intensity of radiation at microwave wavelengths thermally emitted by a surface is generally expressed as a brightness temperature, or T_B. Neglecting atmospheric and outer space contributions, the T_B measured by a passive microwave radiometer at satellite height follows the relationship $T_B = \varepsilon T_S$, where ε is the emissivity of the surface and T_S is its physical temperature in degrees, Kelvin. The proportionality of T_B to T_S is a consequence of the Reyleigh-Jeans approximation to Planck's Law of Thermal Radiation Emission. In reality, most objects emit only a fraction of the radiation that would be emitted by a blackbody at the same physical temperature. The emissivity of a surface medium is strongly dependent on its physical properties and state; important information on the latter can be thus be derived from measurements of TB from space. Due to the inherently poor spatial resolution of passive microwave system, the measured brightness temperature represents an integrated value for all the constituent brightness temperature with the IFOV (instantaneous field of view) or pixel (picture element).

Passive microwave observations of the polar oceans have proved themselves enormously useful in delineating ice edges and in estimating the concentrations of sea ice by virtue of the large contrast between the microwave emissivities of open water and sea ice. Microwave remote sensing is also invaluable as a tool for classifying sea ice, exploiting the fact that brine distribution and state within a given floe depend on the rate at which the ice grew, its age, crystalline structure, temperature profile and its thermodynamic history. Due to its unique dielectric properties, the present of brine in the freeboard layer affects the microwave emissivity and thus the measured brightness temperature. The highly variable and inhomogeneous nature of sea ice renders it a far more complex microwave medium than snow and terrestrial ice; the interpretation of these data is accordingly more complicated.

The determination, both analytically and experimentally, of the bulk dielectric properties of sea ice is a prerequisite to the development of scattering and emission models to aid in the interpretation of satellite microwave data. This challenging field is occupying a number of workers in both experimental and theoretical research, and in studies of both passive (and active) microwave behaviour of sea ice.

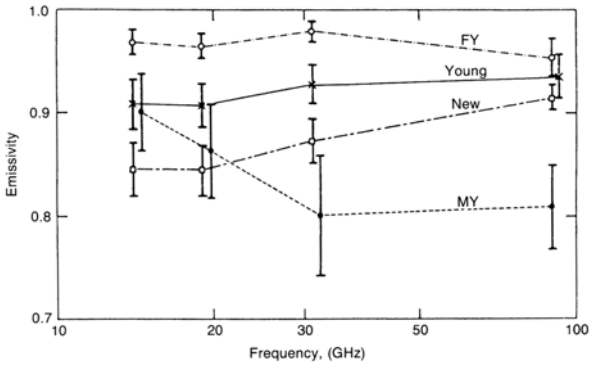

Figure 7.3- The emissivity of four Arctic sea ice types at nadir in the 14-90GHz range. Each vertical bar represents 1 standard deviation in the data, with symbols displaced to avoid overlapping (Troy and others, 1981).

In the central Arctic, the IFOV of a radiometer is generally filled with a mixture of first year (FY) and multi-year (MY) ice (together with many younger and intermediate ice types). First year ice typically has a thickness of > 30cm, and, critically in terms of microwave

remote sensing, is relatively saline in the freeboard layer and has a small penetration depth (typically < 1 wavelength of the observed radiation at a temperature of about -10°C) and thus a high emissivity (assuming that snow cover effects are negligible). Multi-year ice (i.e. ice that has survived at least one melt season) is generally thicker and more deformed, and the brine in its surface layers has been largely flushed away during periods of melt to be replaced to a large extent by air/gas pockets and ice lenses. Being of the sub-millimetre scale, and on sub-centimetre spacing scale similar to the wavelengths of the measured radiation, these enlarged un-homogeneities act as volume scatterers and suppress the effective emissivity of the radiating portion of the ice. Multi-year ice is thus characterised by a relatively low absorption coefficient, a large penetration depth and a correspondingly lower emissivity and brightness temperature. The latter tends to be strongly frequency-dependent, the difference in brightness temperature between FY and MY ice increasing with decreasing wavelength in winter (Fig. 7.3). As a general rule of thumb, the emissivity of sea ice (with a dry snow cover that is transparent to microwave) decreases with increasing density, decreasing salinity, decreasing temperature and brine channel scattering.

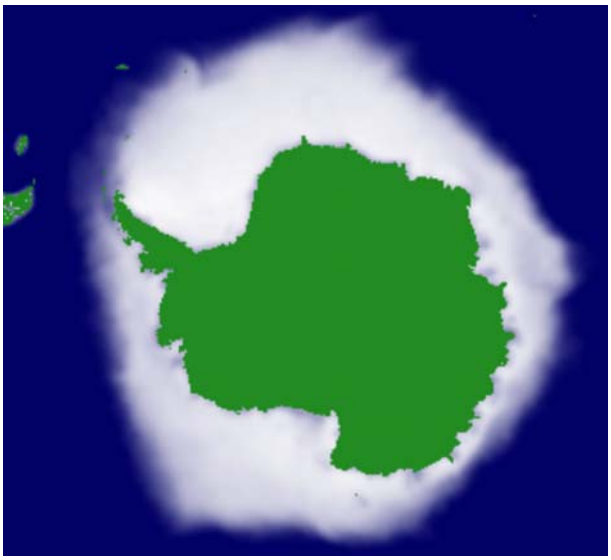

Figure 7.4a- August, Southern Hemisphere.

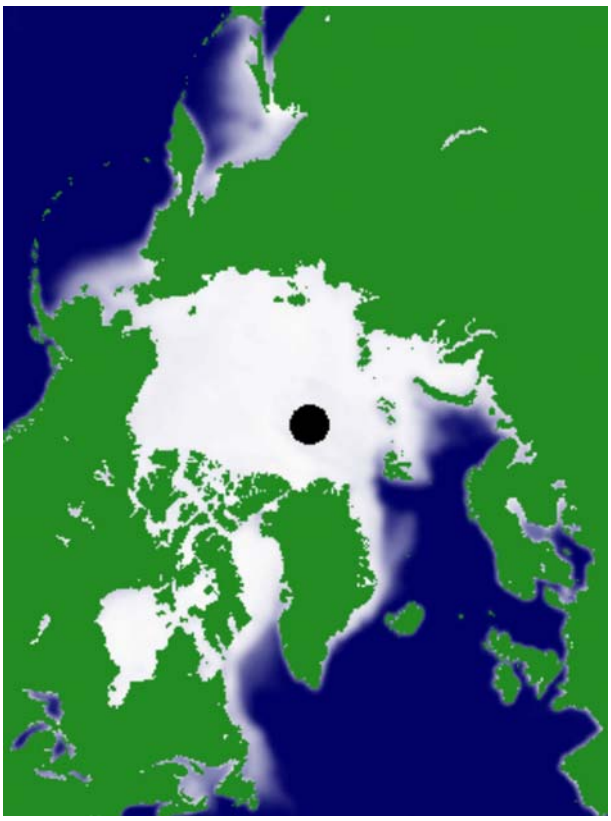

Figure 7.4b- February, Northern Hemisphere.

Figure 7.4- Monthly average sea ice concentrations from the SMMR and SSM/I instruments. The original data were obtained from the National Snow and Ice Data Centre (NSIDC).

During the spring/summer melt period, weathering and ablation processes act on angular surface features to produce a more rounded topography. Snow melts on FY ice in early summer produce a patchy melt water distribution, the low albedo of which causes further locally preferential melting. This process continues until autumn freeze-up and results in an undulating surface relief with patches of refrozen, relatively non-saline melt ponds. Each succeeding melt season enhances the relief on the ice surface, with hummocks becoming higher and melt ponds fewer, until it reaches equilibrium after a number of years.

Polarization effects in passive microwave radiometry of sea ice are poorly understood, yet their analysis may yield additional infor-

mation in the nature of the surface. In general, the brightness temperatures of smooth surfaces display a polarization effect. The observation of both polarizations enhances the distinction of open water from sea ice. Vertically polarized (V) brightness temperatures are invariably greater than those measured at horizontal (H). The contrast between ice and water is greater with H polarization, and increases with increasing wavelength, although this polarization is more sensitive to surface roughness effects. Moreover, the different between the V and H brightness temperature is consistently greater for open water than for all ice types at all microwave frequencies.

7.5 Active Microwave Observations

Active microwave (radar) techniques, whether imaging (real and synthetic aperture radars) or non-imaging (scatterometers and radar altimeters), measure the power backscattered from a surface; a high return results in a bright target on an imaging radar. The important parameters are the backscattering coefficient (expressed in dB), which is related to the emissivity and the penetration depth (both of which have already been discussed). Thus, the electromagnetic properties which are important in active microwave observations are similar to those in passive microwave radiometry. Because of significant remaining uncertainties in the dependence of backscattering coefficient on physical parameters, the main use of imaging radar to date has been in establishing the two-dimensional geometry of ice masses, by making use of radiometric and tonal/textual contrast.

The interpretation of the SAR (Synthetic Aperture Radar) image is not as straightforward as it seems, as volume scattering and/or surface roughness effects may contribute significantly to the detected signal. Surface roughness effects are a function of wavelength, polarization and viewing angle. Attempt to classify sea ice and to infer surface characteristics of land ice have met with limited success, and will require substantially more research before they can be routinely applied. Thanks to the launch of suite of important SARs in the 1990's, however, the research effort has intensified.

SAR imagery is often characterized by random tonal variations from one pixel to the next, a phenomenon known as speckle. This grainy appearance is due to interferences of coherent radiation reflected by neighbouring regions with the same scene. SAR generates images by coherent processing of scattered signals, thereby making it particularly susceptible to speckle noise. Brighter areas are much noisier than darker areas on the image. This factor, alone or in combination with topographic and geometrical effects such as shadows, layover and highlights, can hinder unambiguous interpretation.

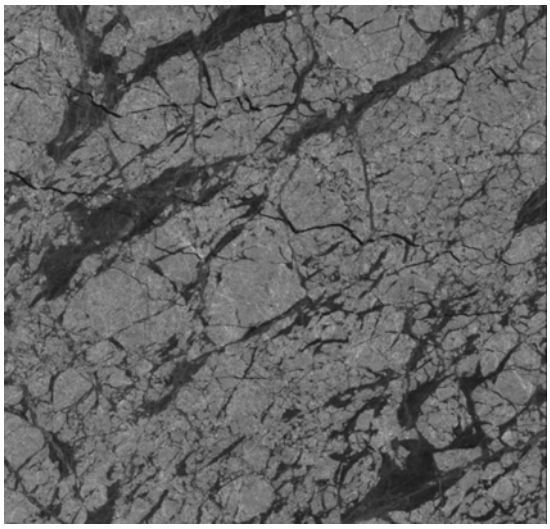

Figure 7.5- ERS-1 SAR image of sea ice. Bright grey regions are sea ice and the brightness corresponds to ice thickness. Black lines between sea ices are open water cracks. Dark grey regions are new ice. (ESA)

7.6 Advanced Microwave Scanning Radiometer – EOS (AMSR-E) Sensor

The most consistent source of sea ice data continues to be satellite passive microwave sensors. Visible and infrared satellite data are

not as useful because coverage is limited by persistent cloud cover, but nevertheless, they have higher resolution and have used for meso-scale studies on surface temperature, albedo, and cloud. Detailed characterization of sea ice under all weather conditions has recently been provided by the SAR data, but only a small fraction of the entire ice cover can be monitored at a time because of operational and data acquisition constraints and a narrow swath width (100 km). Radarsat data with its wider swath (500 km) is an improvement but adequate temporal resolution is still lacking. Such data are nonetheless useful for regional studies and may provide information to improve the interpretation of passive microwave data.

The first passive microwave sensor used extensively for studying the global distribution of sea ice was the Electrically Scanning Microwave Radiometer (ESMR) on board the NASA Nimbus 5 satellite. The ESMR sea ice algorithm was based on a linear relationship between the radiometric brightness temperatures of ice-free water and consolidated sea ice. The Scanning Multi-channel Microwave Radiometer (SMMR) was launched on the SeaSat satellite in July 1978 and on the Nimbus-7 satellite in October 1978. With its multi-channel capability, SMMR provided more information about the ice cover than ESMR. Multi-channel SMMR algorithm provided an opportunity to derive sea ice concentrations more accurately.

In 1987, the first in a new series of passive microwave radiometers was launched as part of the Defence Meteorological Satellite Program (DMSP). This sensor, called the Special Sensor Microwave/Imager (SSMI), operates at frequencies ranging from 19.4 GHz to 85.5 GHz. The SSMI measures both horizontally and vertically polarized components at all frequencies except at 22.2 GHz for which only a vertically polarized component is obtained. Using these data, several new algorithm improvements have been made.

The AMSR-E (Advanced Microwave Scanning Radiometer - EOS) sensor, which is a one of the six sensors aboard Aqua launched on May 4, 2002, is a conically scanning total power passive microwave radiometer sensing microwave radiation (brightness temperatures) at 12 channels and 6 frequencies ranging from 6.9 to 89.0 GHz. Horizontally and vertically polarized radiation are measured separately at each frequency. The AMSR-E system will be a significant improvement over previous and current passive microwave systems. The most obvious improvements are its finer spatial resolution and its wider spectral range. The AMSR-E sea ice algorithm will provide daily maps of sea ice concentration and sea ice temperature, and 5-day-averaged maps of snow depth.

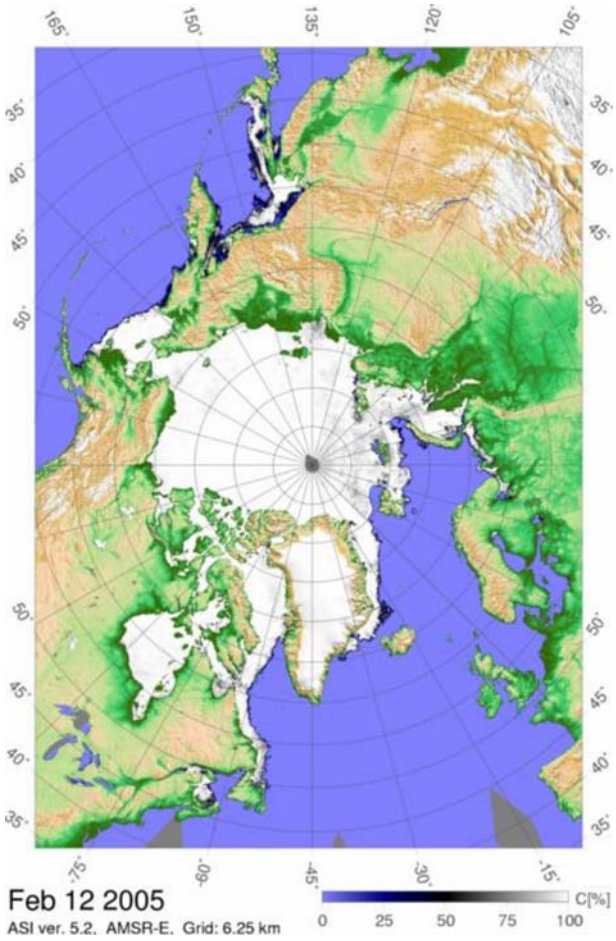

Figure 7.6a- Northern Hemisphere.

The sea ice concentration products will be generated using two algorithms: the enhanced NASA Team (NT2) algorithm and the AMSR Bootstrap algorithm (ABA). In the Arctic, the

NT2 algorithm will be used to obtain the standard sea ice concentration, whereas in the Antarctic, the ABA algorithm will provide the standard product. In addition, the ABA-NT2 and the NT2-ABA ice concentration differences will be provided for the Arctic and Antarctic, respectively. Sea ice temperature is a by-product of the ABA algorithm and the sea ice snow depth will be obtained from an algorithm described by Markus and Cavalieri (1998). The theoretical bases of these algorithms are described in the Algorithm Theoretical Basis Document (Cavalieri and Comiso, 2000).

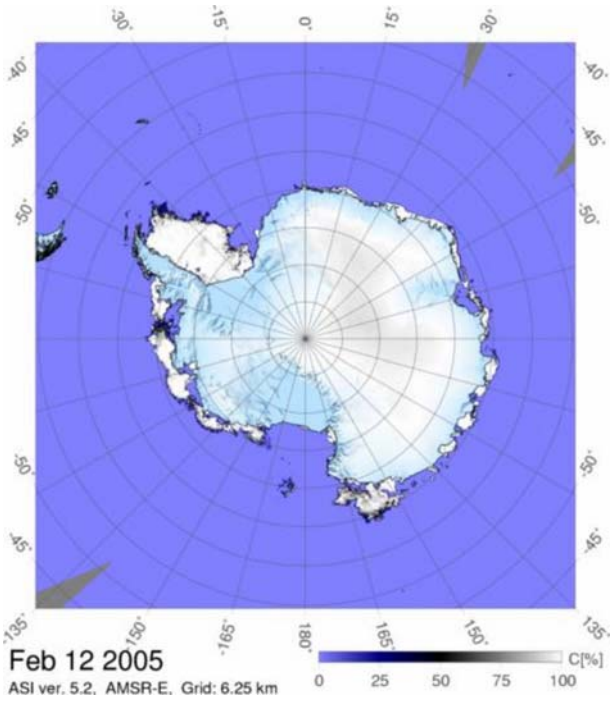

Figure 7.6b- Southern Hemisphere.

Figure 7.6- Sea ice concentrations from the 89 GHz AMSR-E channels using the ARTIST (Arctic Radiation and Turbulence Inter action Study) sea ice algorithm (IUP, University of Bremen). These results are preliminary because AMSR-E is still in the calibration phase, and because they have been produced with the ASI algorithm fine tuned for the SSM/I frequencies.

The principal sea ice parameter derived from AMSR-E brightness temperatures is sea ice concentration. Historically, the two basic assumptions made in the development of sea ice concentration algorithms are (1) that the received radiation by the satellite sensor comes from ocean surfaces: sea ice (I), and ice-free (open) water (W), and (2) that the atmospheric contribution is approximately constant. Using a linear mixing formulation, the received radiation expressed as a function of the brightness of temperature is given by:

$$T_B = T_{Bw} * C_w + T_{BI} * C_r \qquad (7.1)$$

where,
T_{BW} and T_{BI} are the brightness temperatures of ice free ocean and sea ice. C_W and C_I are the corresponding fractions of each of the two ocean surface components within the field-of-view of the instrument and add to unity. The two sea ice concentration algorithms described make use of Eq. (7.1), but the sets of channels and the form of the algorithms used to derive C_I are different.

7.7 Numerical Models for Sea Ice

Many public organizations of countries in high latitude have provided sea ice information. Some of them have provided sea ice forecast as well as current sea ice information. It is largely attributable to the development of sea ice models and a computer in recent years. There are two categories of sea ice model. Sea ice is generated by freezing up water of ocean surface and returns to water by melting. In the meantime, it drifts, breaks up and laps each other. In numerical model for sea ice, these four processes of generation, melting, drift and deformation of sea ice have been described. Thermodynamic model treats the process of heat transfer among sea ice, air and ocean. Sea ice generation and melting are modelled in this process. An earlier thermodynamic model is Maykut and Understeinner model (1971). Hibler (1979) and Parkinson and Washington (1979) models are famous. The latter focuses on the global climate change. The other is dynamic model that expresses sea ice drift and deformation. Many systems for sea ice forecast

are based on the viscous-plastic rheology model developed by Hibler (1979). Hibler's model has treated sea ice as a continuum, therefore it is suitable for sea ice simulation of a wide area. The DMDF (Distributed Mass / Discrete Floe) model developed by Rheem (1994) can express the discrete nature of sea ice for which is difficult to use a continuum model, it is useful for narrow and middle scale simulation of sea ice.

7.8 Summary

Satellite remote sensing is the most powerful technique to collect sea ice information. The most consistent source of sea ice data continues to be satellite passive microwave sensors. Visible and infrared satellite data are not as useful because coverage is limited by persistent cloud cover. Detailed characterization of sea ice has been provided by SAR data, but only a small fraction of the entire ice cover can be monitored at a time and its cost is very high.

The sea ice concentration would be provided by AMSA-E in the near future, but some more time for ice thickness information by satellite remote sensing is needed. Many efforts for improvement in Satellite remote sensing of sea ice are continuing at this moment. At the present, sea ice data provided by satellite remote sensing is base on all sea ice information in the world.

8. TASK 4: CONDUCT TESTS TO DEVELOP AN UNDERSTANDING FOR THE PERFORMANCE OF OPEN WATER PROPELLERS IN ICE

8.1 Introduction

In the literature, many full-scale measurements of the interactions between ice and propellers have been presented (Laskow, 1986; Jussila and Koskinen, 1989; Keinonen et al., 1990; Williams et al., 1992; Cowper et al., 1992). Also as a part of a Joint Research Project Arrangement (JRPA #6), the interaction between ice and propellers was studied from both theoretical and experimental points of view (Keinonen et al., 1990; Jussila and Soininen, 1991; Newbury et al., 1993, 1994; Browne, 1997; Jones et al., 1997). Several model tests in the ice tank were carried out as well (Searle et al., 1999; Soininen, 1998; Moores et al., 2002, Moores, 2002).

Moores et al. (2001) tested a highly skewed propeller and measured the forces and moments due to ice acting on a single blade and Searle et al. (1999) tested both an R-Class icebreaker propeller and a highly skewed propeller. Moores et al. (2001) tests were the first successful tests to accurately measure blade loads during ice milling using a sophisticated dynamometer which was designed to accurately distinguish blade load components: Also, several numerical and empirical studies have been carried out to try and understand the ice loads acting on a propeller blade (Veitch, 1995; Jones et al., 1997; Soininen, 1998).

The tests presented in this report were conducted to develop a better understanding for the behaviour of open water propellers under the ice sheet (blockage effects). The same series of tests were conducted at the IOT/NRC, Canada, and at the Helsinki University of Technology (HUT), Finland. The analysis of the results from both laboratories is still in progress. The detailed analysis will be reported during the next ITTC. However, a preliminary description of the test program, sample of test results, and initial analysis of the results are given in the following subsections.

8.2 Objectives and Test Program

Two series of ice tank experiments were carried out on a model for podded propulsor at the IOT/NRC ice tank test facility (Fig. 8.1) in September 2004 and in March 2005. A picture

and a sketch for the propulsor used in the tests are given in Figs. 8.2a and 8.2b, respectively.

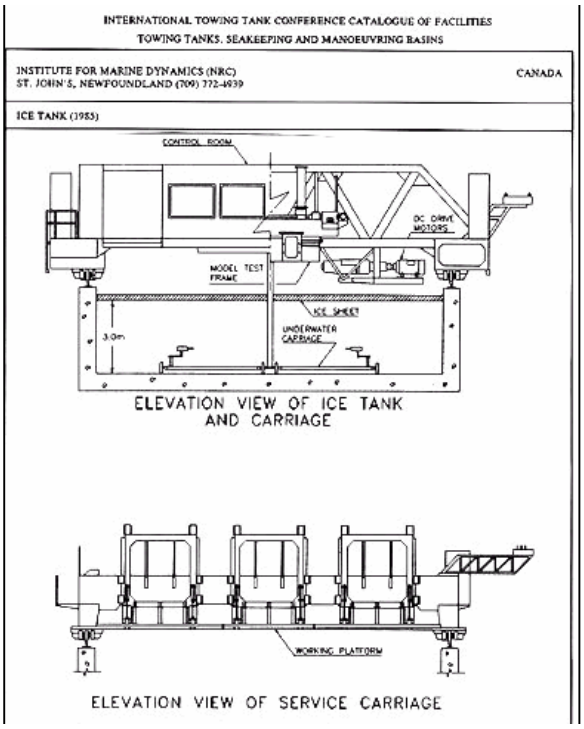

Figure 8.1- Drawing for the IOT/NRC ice tank.

Figure 8.2a- IOT/NRC Test set up.

The data from these tests has been used investigate the performance of a podded propulsor as its propeller approaches the ice sheet from beneath. The objective of the test program is to quantify the effects of the distance between the propeller and the ice sheet on the performance parameters such as the thrust and torque coefficients (Kt and Kq, respectively).

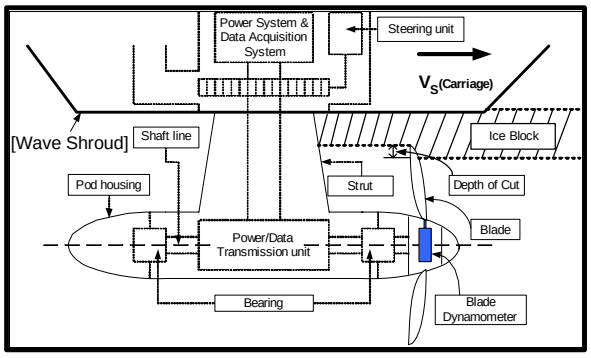

Figure 8.2b- Apparatus of the Puller mode with 180 degree of Azimuthing angle.

8.3 Model Propulsor

The model propulsor had four six-component dynamometers installed to measure blade loads on one blade, shaft-bearing loads and the loads on the whole podded propulsor. The experiments were conducted both in "Pusher" and "Puller" configurations and in various ice conditions. In addition, the rotational speed of the propeller, forward velocity and the azimuthing angle were varied systematically.

Table 8.1- Example for the properties of model ice at random locations.

Depth of Cut	Sample No.	Flexural Strength (kPa)	Comp. Strength (kPa)	Shear Strength (kPa)	Young's Modulus (MPa)	Density (kg/m^3)	Thickness (mm)
35 mm	1	90.0	234.8	114.6	181.5	931.3	57.3
	2	74.7	193.1	90.4		926.3	
	3	63	136.7	70.5			
	Mean	65	195	95	182	929	57
15mm 22mm	1	64.6	223.9	106.0	129.9	930.4	47.4
	2	56.0	164.1	76.3			
	3	43.6	138.0	66.8			
	Mean	55	167	77	130	930	47

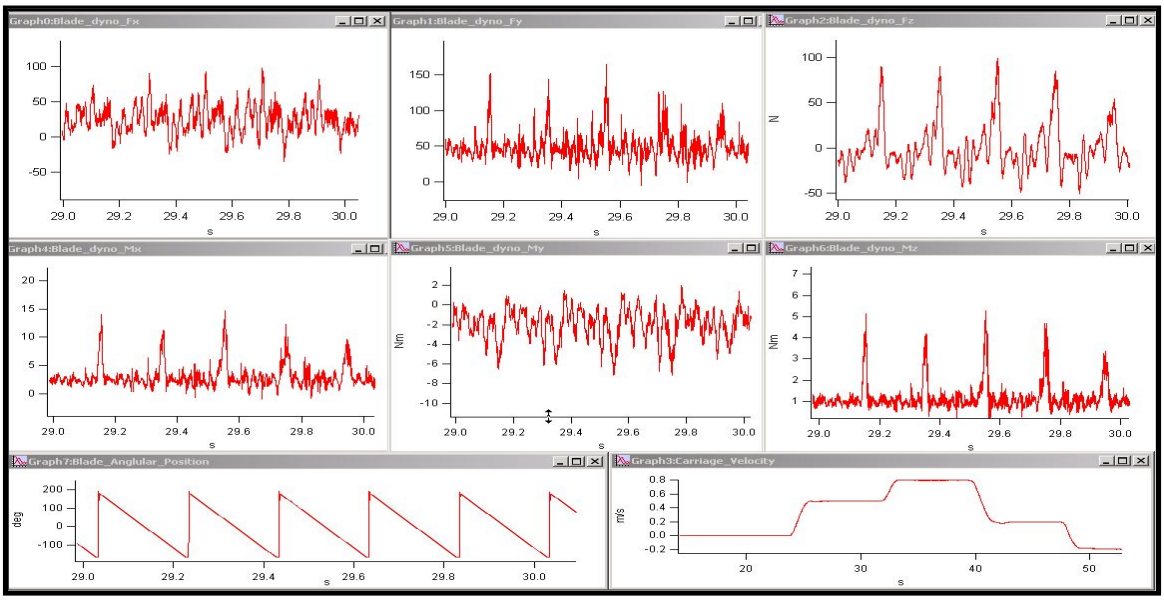

Figure 8.3- Time series data from one of the experimental tests.

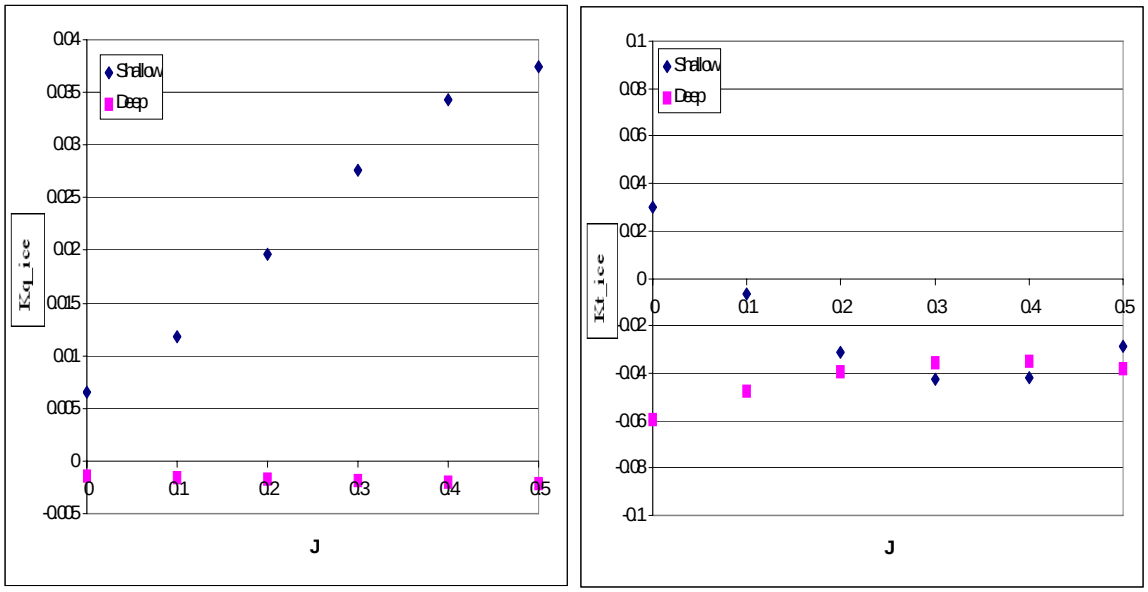

Figure 8.4- Differences in K_t and K_Q due to the presence of ice - both K_t and K_Q are presented as function of the advance coefficient, J.

The propeller was designed to be similar to a general icebreaker propeller. It has a diameter of 0.3 m and four blades. Mean-pitch/diameter ratio (P/D) is 0.76 and expanded blade area ratio (EAR) is 0.669. The diameter of the hub at the propeller is 0.11 m.

During the tests, ice properties were recorded approximately every two hours. An example for ice properties is given in Table 8.1. The experiments were carried out at three different depths, three different carriage velocities, and three different RPS (Rotation per Second) values in both air and water.

8.4 Test Matrix

Tests were performed at different depths, RPS (rounds per second), and carriage velocities (V). In some cases, several runs were

repeated N times. The test matrix is given in Table 8.2.

Depth, mm	RPS	V, m/s	N
35	5, 7, 10	0.2, 0.5, 0.8	
15	5, 7	0.2, 0.5, 0.8	3
22 (in air)	5, 7, 10	0.2, 0.5	

Table 8.2- Test Matrix.

8.5 Typical Test Results

Figure 8.3 shows typical time series data from one of the tests. The upper three graphs show the forces in 3 directions (F_X, F_Y, and F_Z). The middle three graphs show the moments in three directions (M_X, M_Y and M_Z.). The bottom two graphs show the blade angular position and carriage velocity respectively. These graphs are plotted over a one second time interval, 29th to 30th seconds, except for the carriage velocity graph. In the forces and moments graphs, five peaks can be seen because the propeller was rotating at 5 rps and the loads presented are for the "key" blade only. The carriage speed for these graphs was 0.5 m/s.

8.6 Preliminary Analysis

The analysis of the test results is still continuing. In order to quantify the effects of the presence of the ice sheet, the results of the clear water tests were subtracted from the corresponding ice tests.

Figure 8.4 presents the differences in Kt and K_Q due to the presence of ice (both K_t and K_Q are presented as function of the advance coefficient, J). It was expected that in the deeper submerged case, the difference between the clear water and ice tests is minimum. This is indeed the case for K_Q. However, K_t presents a different case. Further experiments and in depth analysis are needed. These initial results suggest that a propeller (and the pod) approaching an ice sheet from beneath may experience variations in their performance.

The analysis of the results of all tests from both laboratories (IOT and HUT) should be combined and used to develop a procedure of testing of podded propellers in ice for the next (25th) ITTC.

9. TASK 5: QUESTIONNAIRE FOR THE USE OF NUMERICAL METHODS APPLIED TO ICE ENGINEERING

9.1 General Aspects

Question 1: Does your Company/Institute (C/I) deal with research, engineering and/or consulting on problems related to (sea) ice, ships and/or structures in ice?

- Ice research in general Y/N
- Physical ice model testing Y/N
- Mechanical properties of ice Y/N
- Engineering for ships in ice Y/N
- Engineering for structures in ice Y/N
- Ice routing Y/N
- Satellite ice observation Y/N

Question 2: Does your C/I develop and/or apply computer codes and numerical methods for ice engineering problems?

- C/I develops codes Y/N
- C/I applies own codes Y/N
- C/I uses commercial codes Y/N
- C/I applies no code Y/N

Question 3: If your C/I develops own computer codes, how many persons are involved?

- Scientists #
- IT personal with expertise in ice #
- IT personal w/o expertise in ice #

9.2 Specific Aspects

Please provide information for each of the following type of codes (Type 1 to 7):

- Code name:
- Purpose of code:
- Theory (ies) involved in the code:
- Validation against model test and/or full scale measurements:
- Publications related d to the code:
- Availability of Computer Codes:

Type 1: Computer codes to determine physical ice properties
Type 2: Computer codes to determine the behaviour of ice under environmental influence (e.g. ice drift scenarios)
Type 3: Computer codes to determine ice loads on (offshore) structures
Type 4: Computer codes to determine ice loads on ships
Type 5: Computer codes to predict icebreaking performance (and manoeuvring) in level ice and other ice conditions
Type 6: Computer codes to predict ice loads on the propulsor (components).
Type 7: Others, please specify

10. CLOSING REMARKS AND GENERAL CONCLUSIONS AND RECOMMENDATIONS

a) It is recommended to develop a procedure for testing of podded propellers in ice: During the 24th ITTC, two series of ice-propeller interaction tests were performed in ice tanks in both Helsinki University of Technology (HUT, Finland) and Institute for Ocean Technology (NRC, Canada). The test results from both laboratories are still being analyzed; they should be combined and used to develop an ITTC procedure for testing of podded propellers in ice.

b) It is recommended to develop a procedure for testing of compliant structures subjected to ice loads: Two universities in China (Dalian University of Technology and Tianjin University) have been working on the development of a realistic method to compute ice loads on compliant "slender" structures, using a cold room (Dalian) and an ice tank (Tianjin), their testing programs focus on ice loads on jacket structures in the Bohai-Sea. Note that Jacket structures have been constructed in ice-infested waters in other parts of the world (such as cook-inlet, Alaska). However, up to now, there is no a procedure or standard that can be followed to test compliant structures in the laboratory. All existing testing methods were developed for rigid structures.

c) It is recommended to develop a procedure for ship tank testing in brash ice. This recommendation came from HSVA. They conducted ship resistance tests in brash ice (The stern of the ship is used for breaking the ice, the ship was equipped with 2 podded propellers). HSVA recommends that their testing program and results should be used to develop a procedure for ship resistance is brash ice.

d) Provide a bibliography for satellite images for sea ice movements and their impact on sea ice modelling in ice tank. Essentially, this is a continuation of the task from the 24th ITTC. During the 24 ITTC, a comprehensive review was done. However, this review was focused mainly on the ice conditions, ice regimes and ice movements in Oshkosh-Sea; Japan. A similar review is needed to cover the Arctic and Sub-Arctic regions (ice infested waters in other parts of the world).

11. REFERENCES

Akinturk, A., Jones, S., Duffy, D., and Rowell, B., 2004, "Ice Loads on Azimuthing podded propulsors", Proc. 23rd OMAE, ASME, New York (CD-ROM, no page numbers).

ASME PTC 19.1, 1998, "Test Uncertainty. Supplement to Performance Test Code, Instruments and Apparatus".

Bose, N., 1996, "Ice Blocked Propeller Performance Prediction Using a Panel

Method", Transactions of the Royal Institution of Naval Architects, Vol. 138.

Browne, R., 1997, "Analysis of Canadian Full Scale Propeller and Ice Interaction Trials Data for Correlation with Empirical Models", Report No. CR-1997-12, Institute for Ocean Technology, National Research Council of Canada.

Canadian Ice Service, CIS, www.ice-glaces.ec.gc.ca

Cavalieri, D. J. and Comiso J. C., 2000, Algorithm Theoretical Basis Document (ATBD) for the AMSR-E Sea Ice Algorithm, Laboratory for Hydrospheric Processes NASA Goddard Space Flight Centre.

Coleman H.W. and Steele W.G., 1998, Experimentation and Uncertainty Analysis for Engineers, 2nd edition, John Wiley & Sons publications, New York.

Cowper, B., Browne, R., Glen, I, and Ritch, R., 1992, "Resistance and Propulsive Performance Trials of the MV Terry Fox and MV Ikaluk in Level Ice", Transactions of the Society of Naval Architects and Marine Engineers, Vol. 100, pp. 315-343.

Derradji-Aouat A., Moores C. and Stuckless S., 2002, "Terry Fox Resistance Tests. The ITTC Experimental Uncertainty Analysis Initiative", IMD report No. TR-2002-01.

Derradji-Aouat A., 2002, "Experimental uncertainty analysis for ice tank ship resistance experiments", IMD/NRC report No. TR-2002-04.

Derradji-Aouat A. and Coëffé J., 2003, "Terry Fox Resistance Tests – Phase II. The ITTC Experimental Uncertainty Analysis", IMD report No. TR-2003-07.

Derradji-Aouat A., 2003, "Phase II Experimental uncertainty analysis for ice tank ship resistance experiments", IMD/NRC report No. TR-2003-09.

Derradji-Aouat A. and van Thiel A., 2004, "Terry Fox Resistance Tests – Phase III (PMM Testing). The ITTC experimental uncertainty analysis initiative", IOT/NRC report No. TR-2004-05.

Derradji-Aouat A., 2004a, "A Method for Calculations of Uncertainty in Ice Tank Ship Resistance Testing", Proc. of the 19th International Symposium on Sea Ice, 2004, pp. 196-206, Mombetsu, Japan.

Derradji-Aouat A., 2004b, "Experimental uncertainty analysis for ship model testing in the ice tank", Proc. of the 25th Symposium on Naval Hydrodynamics, Office of Naval Research, St. John's, Newfoundland and Labrador, Canada, August, 8-13, 2004.

Derradji-Aouat A., Izumiyama K., Yamaguchi H., and Wilkman G., 2004, "Experimental uncertainty analysis for ice tank ship resistance experiments using a model for a Canadian icebreaker *Terry Fox*". Oceanic Engineering International, Vol. 8, No. 2, pp. 49 -69.

European Space Agency, ESA, www.earth.esa.int

GUM., 2003. General Uncertainty Measurements. (http://www.gum.dk/)

Hibler III, W. D., 1979, "A Dynamic Thermodynamic Sea Ice Model", J. Phys. Oceanogr., Vol. 9, pp. 815-846.

ISO., 1995, "Guide to the Expression of Uncertainty in Measurements", ISBN 92-67-10188.

IUP, Bremen, University www.iup.physik.uni-bremen.de:8084/amsr/amsre.html

Japan Aerospace Exploration Agency (JAXA), www.jaxa.jp

Jones, S.J., 1987, "Ice Tank Test Procedure at the Institute for Marine Dynamics", Report No. LM-AVR-20, Institute for Ocean Technology, National Research Council of Canada.

Jones, S.J., Soininen, H., Jussila, M., Koskinen, P., Newbury, S. and Browne, R., 1997, "Propeller-Ice Interaction", Transactions of the Society of Naval Architects and Marine Engineers, Vol. 105, pp. 399-425.

Jussila, M. and Koskinen P., 1989, "Ice Loads on CP-Propeller and Propeller Shaft of Small Ferry and Their Statistical Distributions during Winter '87", 8th International Conference on Offshore Mechanics and Arctic Engineering, Vol. 4, The Netherlands.

Jussila, M. and Soininen, H., 1991, "Interaction between Ice and Propeller", Research Reports 1281, Technical Research of Finland, Espoo.

Kärnä, 2002, "Dynamic ice forces caused by crushing failure", Proc. of the 16th IAHR International Symposium on Ice, Dunedin, New Zealand.

Keinonen, A., Browne, R. and Jacobsen, C., 1990, "Ice propeller interaction forces", Transportation Development Centre Report, TP 10401E.

Laskow, V., Revill, C., 1986, "Engineering Analysis of Ice/Propeller Interaction Data", Transportation Development Centre Report, TP 8450E.

Markus, T. and Cavalieri D. J., 1998, "Snow depth distribution over sea ice in the Southern Ocean from satellite passive microwave data, Antarctic Sea Ice: Physical Processes, Interactions and Variability", Antarctic Research Series, Vol. 74, pp. 19-39, American Geophysical Union, Washington DC.

Massom, R., 1991, Satellite Remote Sensing of Polar Region, Belhaven Press.

Moores, C., Veitch, B., Bose, N., Jones, S. J., Carlton, J., 2002, "Multi-component blade load measurements on a propeller in ice" Transactions Society of Naval Architects and Marine Engineers, Vol. 110, pp. 169-188.

Moores, C., 2002, "Shaft and Blade Load Measurements on a Highly Skewed Propeller Model in Ice" Master of Engineering Thesis, Memorial University of Newfoundland, St. John's, Newfoundland.

National Snow and Ice Data Center (NSIDC), www.nsidc.org

Newbury, S., Shih, L., Browne, R., Revill, C., Kenny, S. and Zheng, Y., 1993, "Experimental and Theoretical evaluation of Hydrodynamic Pressure during Non-Contact Propeller / Ice Interaction", Proc. of the 2nd Canadian Marine Dynamics Conference, Vancouver.

Newbury, S., Browne, R. and Jones, S., 1994, "Experimental Determination of Hydrodynamic Non-Contact loads during Propeller-Ice Interaction", Proc. of ISOPE 94, Osaka, Vol. 2, pp. 596-601.

Parkinson, C. L. and W. M. Washington, A., 1979, "Large-scale Numerical model of sea ice", Journal of Geophysical Research, Vol. 84, pp. 311-337.

Rees, W., 1990, The physical principles of remote sensing, Cambridge University Press.

Rheem, C. K., Yamaguchi H. and Kato H., 1997, Distributed Mass/ Discrete Floe Model for pack ice rheology Computation, J. Mar. Sci. Technol., Vol. 2, pp. 101-121.

Searle, S., Veitch, B., Bose, N., 1999, "Ice-Class Propeller Performance in Extreme Conditions", Transactions Society of Naval

Architects and Marine Engineers, Vol. 107, pp. 127-152.

Soininen, H., 1998, "A propeller-ice contact model", Dissertation for the degree of Doctor of Technology, Helsinki University of Technology, Espoo, 116 p.

Spencer, D.S., and Timco, G.W., 1990, "CD model ice: a process to produce correct density (CD) model ice", Proc. 10th IAHR Symposium on Ice, Espoo, Finland, Vol. 2, pp. 745-755.

Timco, G.., 1986, "EG/AD/S: A new type of model ice for refrigerated towing tanks", Cold Science and Technology, Vol. 12, pp. 175-195.

Troy, B.E., Hollinger, J.P., Lerner, R.M. and Wisler, M.M., 1981, "Measurement of the microwave properties of sea ice at 90 GHz and lower frequencies", Journal of Geophysical Research, Vol. 86-4, pp. 283-9.

Veitch, B., 1995, "Predictions of ice contact forces on a marine screw propeller during the propeller-ice cutting process", Acta Polytechnica Scandinavica, Mechanical Engineering Series, No. 118, Helsinki.

Walker, D., Bose, N., and Yamaguchi, H., 1994a, "Hydrodynamic Performance and Cavitation of an Open Propeller in a Simulated Ice Blocked Flow", Journal of OMAE, Vol. 116.

Wang, J., Akinturk, A., Foster, W., Jones, S.J., and Bose, N., 2004, "An experimental model for ice performance of podded propellers", Proc. of the 27th American Towing Tank Conference, NRC/IOT, (CD-ROM, no page numbers).

Williams, F., Spencer, D., Mathews, S. and Bayly, I., 1992, "Full Scale trials in Level Ice with Canadian R-Class Icebreaker", Transactions of the Society of Naval Architects and Marine Engineers, Vol. 100, pp. 293-313.

Yue, Q.J. and Bi, X.J., 1998, "Full-scale tests and analysis of dynamic interaction between ice sheet and conical structures", Proc. of 14th International Association for Hydraulic Research (IAHR), Vol. II, Symposium on Ice, Potsdam.

Yue, Q.J. and Bi, X.J., 2000, "Ice-induced jacket structure vibrations in Bohai Sea", J. of Cold Regions Engineering (ASCE) 14(2): pp. 81–92.

Yue,Q.,J. Zhang, X., Bi. X., and Shi Z., 2001, "Measurement and analysis of ice induced steady-state vibrations", Proc. of POAC'01, Ottawa, Canada, Vol.1, pp. 413-420.